

PGB pair production at LHC and ILC as a probe of the topcolor-assisted technicolor models

Guo-Li Liu¹, Huan-Jun Zhang², Ping Zhou^{1,3}

¹*Department of Physics, Zhengzhou University, Zhengzhou, China*

²*Department of Physics, Zhengzhou University of Light Industry, Zhengzhou, China*

³*Institut für Strahlenphysik, Forschungszentrum
Dresden-Rossendorf, 01314 Dresden, Germany*

Abstract

The topcolor-assisted technicolor (TC2) model predicts some light pseudo goldstone bosons (PGBs), which may be accessible at the LHC or ILC. In this work we study the pair productions of the charged or neutral PGBs at the LHC and ILC. For the productions at the LHC we consider the processes proceeding through gluon-gluon fusion and quark-antiquark annihilation, while for the productions at the ILC we consider both the electron-positron collision and the photon-photon collision. We find that in a large part of parameter space the production cross sections at both colliders can be quite large compared with the low standard model backgrounds. Therefore, in future experiments these productions may be detectable and allow for probing TC2 model.

PACS numbers: 12.60.Nz, 14.80.Bn

I. INTRODUCTION

It is widely believed that the mechanism of electroweak symmetry breaking(EWSB) and the origin of the particle mass remain prominent mystery in current particle physics in spite of the success of the standard model(SM) tested by high energy experimental data. There has been no experimental evidence of the SM Higgs boson existing. Furthermore, the neutrino oscillation experiments have made one believe that neutrinos are massive, oscillate in flavor, which presently provides the only experimental hints of new physics [1]. Thus, the SM can only be an effective theory below some high energy scales. Other EWSB mechanisms and extended Higgs sectors have not been excluded in the theoretical point of view.

To completely avoid the problems arising from the elementary Higgs scalar field in the standard model (SM), various kinds of models for electroweak symmetry breaking (EWSB) have been proposed, among which the technicolor models[2, 3] are attractive because they provide a possible EWSB mechanism without introducing an elementary scalar Higgs boson. In this kind of models, EWSB can be achieved via introducing new strong interaction. Technicolor models open up new possibilities for new physics beyond the SM, which might produce observed signatures in future high energy collider experiments.

Among various kinds of technicolor theories, the topcolor scenario[4] is attractive because it can explain the large top quark mass and provides a possible EWSB mechanism. The topcolor-assisted technicolor (TC2) model[3] is one of the phenomenologically viable models, which has all essential features of the topcolor scenario. This model predicts three CP-odd top-pions π_t^0 , π_t^\pm and one CP-even top-higgs h_t^0 with large couplings to the third family, which may make these new scalar particles have a distinct experimental signature[5]. Thus, discovery of a doubly scalar particles in future high energy colliders would be a definite signal of new physics beyond the SM, which would help us to understand the scalar sector and more importantly what lies beyond the SM.

The CERN Large Hadron Collider (LHC) has already started its operation, and it will have considerably capability to discover and measure almost all the quantum properties of a standard model (SM) higgs boson of any mass [6]. However, from the theoretical view point, it would be expected that the SM is replaced by a more fundamental theory at the TeV scale. If hadron colliders find evidence for a new scalar state, it may not necessarily be the SM higgs boson. Many alternative new physics theories, such as supersymmetry, technicolor, and little Higgs, predict the existence of new scalars or pseudo-scalar particles. These new particles may have so large cross sections and branching fractions as to be observable at the high energy colliders. Thus, studying the production and decays of the new scalars at hadron colliders, the future international lepton collider and the $\gamma\gamma$ collider will be of special interest.

On the other side, at the tree-level or one-loop level, the scalar pair productions of the new particles predicted in the new physics model may have very large production rates [7], so it may be interesting to consider the pair production of the new scalars and analysis the observable possibility in TC2 model. We hope that SS' (S , S' denotes any one of the new scalars, i.e, top-pions π_t^0 , π_t^\pm and top-higgs h_t^0) productions can be carried out at the LHC,

the future international linear collider (ILC) and the photon linear collider (PLC) to test the topcolor scenario of the TC2 model.

At the LHC, the measurement of the pair production would be interesting. If we can get larger cross sections surpassing the SM prediction, it would provide a powerful proof to probe the new physics model. At the ILC, A PGB pair can be produced in the process $e^+e^- \rightarrow SS'$, in which the $SS'Z(\gamma)$ coupling can be probed via the new couplings $Z(\gamma)\pi_t^+\pi_t^-$ and $Z\pi_t^0h_t^0$. On the other hand, the PLC option may also be useful to explore the new physics coupling concerning the PGBs. At the second stage of the ILC ($\sqrt{s} = 1.5$ TeV), the signal should increase with the increasing center-of-mass.

In this paper, we study how the technicolor models affect the scalar pair production processes $gg \rightarrow SS'$, $e^+e^- \rightarrow SS'$, $q\bar{q} \rightarrow SS'$ and $\gamma\gamma \rightarrow SS'$, via the new couplings in the TC2 model. Cross sections for these bosons pair production processes are evaluated, and can be significantly large considering the small SM backgrounds. By measuring these double scalar bosons production processes at different collider experiments, we would be able to probe properties of new physics particles, which helps identify the new physics model.

In Sec. II, the technicolor models relative to our calculations are reviewed, and the effects of the new couplings in the scalar boson pair production processes $gg \rightarrow SS'$ and $q\bar{q} \rightarrow SS'$ ($q = u, d, c, s, b$ quarks) at LHC, $e^+e^- \rightarrow SS'$ at the ILC, and $\gamma\gamma \rightarrow SS'$ at the photon collider options, discussed too. Sec. III shows the numerical results for every processes, respectively and analysis the SM backgrounds and the detectable probability for every final state at the different colliders. Summary and discussions are given in Sec. IV.

II. TC2 MODEL AND THE RELEVANT COUPLINGS

To solve the phenomenological difficulties of traditional technicolor(TC) theory, TC2 theory[3] was proposed by combing TC interactions with the topcolor interactions for the third generation at the scale of about 1 TeV.

The TC2 theory introduces two strongly interacting sectors, with one sector (topcolor interaction) generating the large top quark mass and partially contributing to EWSB while the other sector (technicolor interaction) responsible for the bulk of EWSB and the generation of light fermion masses. At the EWSB scale, it predicts the existence of two groups of composite scalars from topcolor and technicolor condensations, respectively [3, 8]. In the linear realization, the scalars of our interest can be arranged into two $SU(2)$ doublets, namely Φ_{top} and Φ_{TC} [8–10], which are analogous to the Higgs fields in a special two-Higgs-doublet model [13]. The doublet Φ_{top} from topcolor condensation couples only to the third-generation quarks. Its main task is to generate the large top quark mass. It can also generate a sound part of bottom quark mass indirectly via instanton effect[3]. Since a small value of the top-pion decay constant F_t (the vacuum expectation value (VEV) of the doublet Φ_{top}) is theoretically favored (see below), this doublet must couple strongly to top quark in order to generate the expected top quark mass. The other doublet Φ_{TC} , which is technicolor condensate, is mainly responsible for EWSB and light fermion masses. It also contributes

a small portion to the third-generation quark masses. Because its VEV V_{TC} is generally comparable with V_W , its Yukawa couplings with all fermions are small. The Yukawa term in the low-energy effective Lagrangian can be written as [10]

$$\mathcal{L}_Y = - \left(\sum_{i,j=1}^3 \lambda_{ij}^U \bar{Q}_{Li} \Phi_{TC} U_{Rj} + \sum_{i,j=1}^3 \lambda_{ij}^D \bar{Q}_{Li} \tilde{\Phi}_{TC} D_{Rj} + Y_t \bar{\Psi}_L \Phi_{top} t_R + h.c. \right) + \dots \quad (1)$$

where Q_{Li} denotes the left-handed quark doublet, U_{Rj} and D_{Rj} are right-handed quarks, Ψ_L is the left-handed top-bottom doublet, $\tilde{\Phi}_{TC}$ is the conjugate of Φ_{TC} , and $\lambda_{ij}^{U,D}$ and Y_t are Yukawa coupling constants satisfying $\lambda_{ij}^{U,D} \ll Y_t$. The two $SU(2)$ doublets take the form

$$\Phi_{TC} = \begin{pmatrix} V_{TC} + (H_{TC}^0 + i\Pi_{TC}^0)/\sqrt{2} \\ \Pi_{TC}^- \end{pmatrix}, \quad (2)$$

$$\Phi_{top} = \begin{pmatrix} F_t + (H_{top}^0 + i\Pi_{top}^0)/\sqrt{2} \\ \Pi_{top}^- \end{pmatrix}. \quad (3)$$

We can rotate the two doublets into $\Phi_{1,2}$ such that $\langle \Phi_1 \rangle = \sqrt{V_{TC}^2 + F_t^2} = V_W$ and $\langle \Phi_2 \rangle = 0$

$$\Phi_1 = (\cos \beta \Phi_{TC} + \sin \beta \Phi_{top}) = \begin{pmatrix} v_w + (H_1^0 + iG^0)/\sqrt{2} \\ G^- \end{pmatrix}, \quad (4)$$

$$\Phi_2 = (-\sin \beta \Phi_{TC} + \cos \beta \Phi_{top}) = \begin{pmatrix} (H_2^0 + iA^0)/\sqrt{2} \\ H^- \end{pmatrix}, \quad (5)$$

where $\tan \beta = F_t/V_{TC}$. Then the Lagrangian can be rewritten as

$$\begin{aligned} \mathcal{L}_Y = & - \left(\sum_{i,j=1}^3 \lambda_{ij}^U \bar{Q}_{Li} \Phi_1 U_{Rj} + \sum_{i,j=1}^3 \lambda_{ij}^D \frac{\sqrt{V_W^2 - F_t^2}}{V_W} \bar{Q}_{Li} \tilde{\Phi}_1 D_{Rj} - \sum_{i,j=1}^3 \lambda_{ij}^D \frac{F_t}{V_W} \bar{Q}_{Li} \tilde{\Phi}_2 D_{Rj} \right. \\ & \left. - \sum_{i,j=1}^3 \lambda_{ij}^U \frac{F_t}{V_W} \bar{Q}_{Li} \Phi_2 U_{Rj} + Y_t \frac{\sqrt{V_W^2 - F_t^2}}{V_W} \bar{\Psi}_L \Phi_2 t_R + h.c. \right) + \dots \end{aligned} \quad (6)$$

where $\lambda_{ij}^U = \lambda_{ij}^U \cos \beta + Y_t \sin \beta \delta_{i3} \delta_{j3}$. In this new basis, G^\pm and G^0 are Goldstone bosons while the pseudoscalar A^0 , the charged scalar H^\pm and the CP-even scalars $H_{1,2}^0$ are physical PGBs. It is obvious that H_1^0 plays the role of the "standard" Higgs boson with flavor diagonal couplings and H_2^0 decouples from the SM vector bosons but has strong coupling only with top quark. In our following analysis, we will adopt the same notations as in the literature, i.e., using top-Higgs h_t^0 , top-pions $\pi_t^{0,\pm}$ to denote H_2^0 , A^0 and H^\pm , respectively.

In Eq.(6), the rotation of quarks into their mass eigenstates will induce FCNC Yukawa interactions from the Φ_2 couplings¹. Since $\lambda_{ij}^{U,D} \ll Y_t$, the FCNC couplings from λ_{ij}^U and λ_{ij}^D

¹ Just like the Higgs field in the SM, Φ_1 terms give no FCNC couplings since they are diagonalized simultaneously with the fermion mass matrices.

can be safely neglected. Because $Y_t = (1 - \epsilon)m_t/F_t$ (ϵ denoting the fraction of technicolor contribution to the top quark mass) is quite large (about $2 \sim 3$) and the mixing between c_R and t_R can be naturally as large as 30% [12], the FCNC coupling from the Y_t term may be sizable and thus may have significant phenomenological consequence. The FCNC couplings from this term are given by

$$\mathcal{L}_{FCNC} = \frac{(1 - \epsilon)m_t}{\sqrt{2}F_t} \frac{\sqrt{v_w^2 - F_t^2}}{v_w} \left(iK_{UL}^{tt*} K_{UR}^{tt} \bar{t}_L t_R \pi_t^0 + \sqrt{2} K_{UR}^{tt*} K_{DL}^{bb} \bar{t}_R b_L \pi_t^- + iK_{UL}^{tt*} K_{UR}^{tc} \bar{t}_L c_R \pi_t^0 \right. \\ \left. + \sqrt{2} K_{UR}^{tc*} K_{DL}^{bb} \bar{c}_R b_L \pi_t^- + K_{UL}^{tt*} K_{UR}^{tt} \bar{t}_L t_R h_t^0 + K_{UL}^{tt*} K_{UR}^{tc} \bar{t}_L c_R h_t^0 + h.c. \right), \quad (7)$$

where K_{UL} , K_{DL} and K_{UR} are the rotation matrices that transform the weak eigenstates of left-handed up-type, down-type and right-handed up-type quarks to their mass eigenstates, respectively. According to the analysis of [12], their favored values are given by

$$K_{UL}^{tt} \simeq K_{DL}^{bb} \simeq 1, \quad K_{UR}^{tt} \simeq \frac{m'_t}{m_t} = 1 - \epsilon, \quad K_{UR}^{tc} \leq \sqrt{1 - (K_{UR}^{tt})^2} = \sqrt{2\epsilon - \epsilon^2}, \quad (8)$$

with m'_t denoting the topcolor contribution to the top quark mass. In Eq.(7) we neglected the mixing between up quark and top quark.

Using the same scalar SU(2) doublets in Eq. (2),(3), the kinetic term is

$$\mathcal{L}_{kin} = \left(D_\mu \Phi_{TC} \right)^\dagger \left(D^\mu \Phi_{TC} \right) + \left(D_\mu \Phi_{top} \right)^\dagger \left(D^\mu \Phi_{top} \right), \quad (9)$$

The covariant derivative is

$$D_\mu = \partial_\mu + i \frac{g'Y}{2} B_\mu + i \frac{g}{2} \tau_i W_\mu^i. \quad (10)$$

The hypercharge of the doublets is $Y = -1$. We make the following redefinition of fields:

$$W_\mu^\pm = \frac{1}{\sqrt{2}} (W_\mu^1 \mp i W_\mu^2), \quad (11)$$

$$W_\mu^3 = Z_\mu \cos \theta + A_\mu \sin \theta, \quad (12)$$

$$B_\mu = -Z_\mu \sin \theta + A_\mu \cos \theta. \quad (13)$$

After replacement of the physical vector boson fields, the $D_\mu \Phi_i$ term for each doublet will be of the form

$$D_\mu \Phi_i = \left(\begin{array}{c} \frac{1}{\sqrt{2}} (\partial_\mu H_i + i \partial_\mu \Pi_i^0) \\ i \partial_\mu \Pi_i^- \end{array} \right) + \frac{ig_Z}{2} Z_\mu \left(\begin{array}{c} \frac{1}{\sqrt{2}} (v_i + H_i + i \Pi_i^0) \\ -i(1 - 2 \sin^2 \theta_W) \Pi_i^- \end{array} \right) \\ + e A_\mu \left(\begin{array}{c} 0 \\ \Pi_i^- \end{array} \right) + \frac{ig}{2} \left(\begin{array}{c} i \sqrt{2} W_\mu^+ \Pi_i^- \\ W_\mu^- (v_i + H_i + i \Pi_i^0) \end{array} \right). \quad (14)$$

where $g_Z = g/\cos \theta_W$ and $e = g \sin \theta_W$. After expanding the terms in Eq. (9), we form orthogonal linear combinations of the fields $\Pi_i^{0,\pm}$,

$$G^{0,\pm} = \frac{F_t \Pi_{top}^{0,\pm} + V_{TC} \Pi_{TC}^{0,\pm}}{V_W} \quad (\text{Goldstone bosons}), \quad (15)$$

$$\pi_t^{0,\pm} = \frac{V_{TC}\Pi_{top}^{0,\pm} - F_t\Pi_{TC}^{0,\pm}}{V_W} \quad (\text{physical top} - \text{pions}). \quad (16)$$

After rearrangement the Feynman rules can simply be read off, however, Table I lists only the 3-point gauge couplings for the physical fields relative to our calculation.

$Z^\mu h_t^0 \pi_t^0$	$-\frac{ig_Z}{2} \frac{V_{TC}}{V_W} (p_\mu^h - p_\mu^0)$	$A^\mu \pi_t^- \pi_t^+$	$e (p_\mu^- - p_\mu^+)$
$Z^\mu \pi_t^- \pi_t^+$	$g_Z (1 - 2 \sin^2 \theta_W) (p_\mu^- - p_\mu^+)$	$W^{-\mu} \pi_t^0 \pi_t^+$	$-\frac{g}{2} (p_\mu^0 - p_\mu^+)$
$W^{-\mu} h_t^0 \pi_t^+$	$-\frac{ig}{2} \frac{V_{TC}}{V_W} (p_\mu^h - p_\mu^+)$	$W^{+\mu} \pi_t^- h_t^0$	$\frac{ig}{2} \frac{V_{TC}}{V_W} (p_\mu^- - p_\mu^h)$

TABLE I: 3-point TC2 gauge couplings for the physical fields; All bosons (charge and momentum) flow out.

Now we recapitulate the theoretical and experimental constraints on the relevant parameters.

- (1) About the ϵ parameter. In the TC2 model, ϵ parameterizes the portion of the extended-technicolor (ETC) contribution to the top quark mass. The bare value of ϵ is generated at the ETC scale, and subject to very large radiative enhancement from the topcolor and $U(1)_{Y_1}$ by a factor of order 10 when evolving down to the weak scale [3]. This ϵ can induce a nonzero top-pion mass (proportional to $\sqrt{\epsilon}$) [14] and thus ameliorate the problem of having dangerously light scalars. Numerical analysis shows that, with reasonable choice of other input parameters, ϵ of order $10^{-2} \sim 10^{-1}$ may induce top-pions as massive as the top quark [3]. Indirect phenomenological constraints on ϵ come from low energy flavor-changing processes such as $b \rightarrow s\gamma$ [15]. However, these constraints are very weak. From the theoretical point of view, ϵ with value from 0.01 to 0.1 is favored. Since a large ϵ can slightly suppress the FCNC Yukawa couplings, we fix conservatively $\epsilon = 0.1$ throughout this paper.
- (2) The parameter K_{UR}^{tc} is upper bounded by the unitary relation $K_{UR}^{tc} \leq \sqrt{1 - (K_{UR}^{tt})^2} = \sqrt{2\epsilon - \epsilon^2}$. For a ϵ value smaller than 0.1, this corresponds to $K_{UR}^{tc} < 0.43$. In our analysis, we will treat K_{UR}^{tc} as a free parameter.
- (3) About the top-pion decay constant F_t , the Pagels-Stokar formula [16] gives an expression in terms of the number of quark color N_c , the top quark mass, and the scale Λ at which the condensation occurs:

$$F_t^2 = \frac{N_c}{16\pi^2} m_t^2 \ln \frac{\Lambda^2}{m_t^2}. \quad (17)$$

From this formula, one can infer that, if $t\bar{t}$ condensation is fully responsible for EWSB, i.e. $F_t \simeq V_W \equiv v/\sqrt{2} = 174$ GeV, then Λ is about $10^{13} \sim 10^{14}$ GeV. Such a large value is less attractive since by the original idea of technicolor [2], one expects new physics scale should not be far higher than the weak scale. On the other hand, if one believes that new physics exists at TeV scale, i.e. $\Lambda \sim 1$ TeV, then $F_t \sim 50$ GeV,

which means that $t\bar{t}$ condensation alone cannot be wholly responsible for EWSB and to break electroweak symmetry needs the joint effort of topcolor and other interactions like technicolor. By the way, Eq.(17) should be understood as only a rough guide, and F_t may in fact be somewhat lower or higher, say in the range $40 \sim 70$ GeV. Allowing F_t to vary over this range does not qualitatively change our conclusion, and, therefore, we use the value $F_t = 50$ GeV for illustration in our numerical analysis.

- (4) About the mass bounds for top-pions and top-Higgs. On the theoretical side, some estimates have been done. The mass splitting between the neutral top-pion and the charged top-pion should be small since it comes only from the electroweak interactions [17]. Ref.[3] has estimated the mass of top-pions using quark loop approximation and showed that m_π is allowed to be a few hundred GeV in a reasonable parameter space. Like Eq.(17), such estimations can only be regarded as a rough guide and the precise values of top-pion masses can be determined only by future experiments. The mass of the top-Higgs h_t^0 can be estimated in the Nambu-Jona-Lasinio (NJL) model in the large N_c approximation and is found to be about $2m_t$ [8, 18]. This estimation is also rather crude and the mass below the $t\bar{t}$ threshold is quite possible in a variety of scenarios [19]. On the experimental side, current experiments have restricted the mass of the charged top-pion. For example, the absence of $t \rightarrow \pi_t^+ b$ implies that $m_{\pi_t^+} > 165$ GeV [20] and R_b analysis yields $m_{\pi_t^+} > 220$ GeV [21, 22]. For the neutral top-pion and top-Higgs, the experimental restrictions on them are rather weak. (Of course, considering theoretically that the mass splitting between the neutral and charged top-pions is small, the R_b bound on the charged top-pion mass should be applicable to the neutral top-pion masses.) The current bound on techni-pions [23] does not apply here since the properties of top-pion are quite different from those of techni-pions. The direct search for the neutral top-pion (top-Higgs) via $pp(\text{or } p\bar{p}) \rightarrow t\bar{t}\pi_t^0(h_t^0)$ with $\pi_t^0(h_t^0) \rightarrow b\bar{b}$ was proven to be hopeless at Tevatron for the top-pion (top-Higgs) heavier than 135 GeV [10]. The single production of $\pi_t^0(h_t^0)$ at Tevatron with $\pi_t^0(h_t^0)$ mainly decaying to $t\bar{c}$ may shed some light on detecting top-pion (top-Higgs)[18], but the potential for the detection is limited by the value of K_{UR}^{tc} and the detailed background analysis is absent now. Moreover, these mass bounds will be greatly tightened at the running and the incoming LHC [10, 12, 24], and Ref.[11] has limited the top-pion mass larger than 300 GeV. Combining the above theoretical and experimental bounds, we in our discussion will assume

$$m_{h_t^0} > 300 \text{ GeV} \quad m_{\pi_t^0} = m_{\pi_t^+} \equiv m_{\pi_t} > 220 \text{ GeV}. \quad (18)$$

We, however, in the following calculations will assume the top-Higgs mass equal to that of the top-pion and see the behavior in the assumption.

III. THE PGB PAIR PRODUCTIONS AT COLLIDERS

In this section, we discuss PGB pair production processes $gg \rightarrow SS'$, $q\bar{q}SS'(q = u, d, s, c, b)$, $e^+e^- \rightarrow SS'$ and $\gamma\gamma \rightarrow SS'$ in TC2 model. In these processes, some couplings such as $\pi_t^\pm \bar{b}c$ and $Z\pi_t^+\pi_t^-$, $Z\pi_t^0h_t^0$ etc., contain the model-dependent parameters so that they can be used to probe the new physics theory at future collider experiments.

At the LHC, the cross sections of the PGB pair production comes mainly from the gluon fusion and quark pair annihilation processes $gg \rightarrow \pi_t^+\pi_t^-$, $gg \rightarrow \pi_t^0h_t^0$, $\pi_t^0\pi_t^0$, $h_t^0h_t^0$, $q\bar{q} \rightarrow \pi_t^+\pi_t^-$, $q\bar{q} \rightarrow \pi_t^0h_t^0$, $\pi_t^0\pi_t^0$, $h_t^0h_t^0$ ($q = u, d, s, c, b$), $u\bar{d} \rightarrow \pi_t^+\pi_t^0(h_t^0)$.

Note that for the neutral final states, there could be $\pi_t^0\pi_t^0$, $\pi_t^0h_t^0$ and $h_t^0h_t^0$, the cross sections of which, however, are not the same even if we take m_{h_t} equal to m_π with the same values of the other parameters, and in the following, we will discuss them one by one. It is relevant to calculate separately the cross sections for the $\pi_t^0\pi_t^0$, $\pi_t^0h_t^0$ and $h_t^0h_t^0$, final states because, for equal masses of π_t^0 and h_t^0 , all three of these final states will contribute to the experimental signal, and so it is important to know the cross sections for all three of them.

At the LHC, the parton level cross sections are calculated at the leading order as

$$\hat{\sigma}(\hat{s}) = \int_{\hat{t}_{min}}^{\hat{t}_{max}} \frac{1}{16\pi\hat{s}^2} \overline{\Sigma} |M_{ren}|^2 d\hat{t}, \quad (19)$$

with

$$\hat{t}_{max,min} = \frac{1}{2} \left\{ m_{p_1}^2 + m_{p_2}^2 - \hat{s} \pm \sqrt{[\hat{s} - (m_{p_1} + m_{p_2})^2][\hat{s} - (m_{p_1} - m_{p_2})^2]} \right\}, \quad (20)$$

where p_1 and p_2 are the first and the second initial particles in the parton level, respectively. For our case, they could be gluon g and quarks u, d, s, b etc.

The total hadronic cross section for $pp \rightarrow SS' + X$ can be obtained by folding the subprocess cross section $\hat{\sigma}$ with the parton luminosity

$$\sigma(s) = \int_{\tau_0}^1 d\tau \frac{dL}{d\tau} \hat{\sigma}(\hat{s} = s\tau), \quad (21)$$

where $\tau_0 = (m_{p_1} + m_{p_2})^2/s$, and s is the pp center-of-mass energy squared. $dL/d\tau$ is the parton luminosity given by

$$\frac{dL}{d\tau} = \int_{\tau}^1 \frac{dx}{x} [f_{p_1}^p(x, Q) f_{p_2}^p(\tau/x, Q) + (p_1 \leftrightarrow p_2)], \quad (22)$$

where $f_{p_1}^p$ and $f_{p_2}^p$ are the parton p_1 and p_2 distribution functions in a proton, respectively. In our numerical calculation, the CTEQ6L parton distribution function is used [26] and take factorization scale Q and the renormalization scale μ_F as $Q = \mu_F = 2m_{\pi_1}$. The loop integrals are evaluated by the LoopTools package [27].

At an electron-positron linear collider, the PGB pair production can be realized by $e^+e^- \rightarrow \pi_t^+\pi_t^-$, $e^+e^- \rightarrow \pi_t^0h_t^0$. The $e^+e^- \rightarrow \pi_t^+\pi_t^-$, $\pi_t^0h_t^0$ process may be promising channels

at the ILC for light PGBs because of the simple kinematical structure. Since relatively larger collision energy is required for two top-pion final states of $\pi_t^+\pi_t^-$ and $\pi_t^0h_t^0$, the s -channel nature of the process may decrease the cross section. On the other hand, if we have large enough energy, one can control the collision energy to obtain the maximal production rate.

At a high energy lepton collider, the hard photons can be obtained from the Compton back scattering method [28]. By using hard photons, PGB pairs can be produced in $\gamma\gamma \rightarrow \pi_t^+\pi_t^-$ and $\gamma\gamma \rightarrow \pi_t^0h_t^0$, $\pi_t^0\pi_t^0$ and $h_t^0h_t^0$ processes, the feynman diagrams of which are shown in FIG. 13.

Since the photon beams in $\gamma\gamma$ collision are generated by the backward Compton scattering of the incident electron- and the laser-beam, the events number is obtained by convoluting the cross section of $\gamma\gamma$ collision with the photon beam luminosity distribution:

$$N_{\gamma\gamma \rightarrow \ell_i \bar{\ell}_j} = \int d\sqrt{s_{\gamma\gamma}} \frac{d\mathcal{L}_{\gamma\gamma}}{d\sqrt{s_{\gamma\gamma}}} \hat{\sigma}_{\gamma\gamma \rightarrow \ell_i \bar{\ell}_j}(s_{\gamma\gamma}) \equiv \mathcal{L}_{e^+e^-} \sigma_{\gamma\gamma \rightarrow \ell_i \bar{\ell}_j}(s) \quad (23)$$

where $d\mathcal{L}_{\gamma\gamma}/d\sqrt{s_{\gamma\gamma}}$ is the photon-beam luminosity distribution and $\sigma_{\gamma\gamma \rightarrow \ell_i \bar{\ell}_j}(s)$ (s is the squared center-of-mass energy of e^+e^- collision) is defined as the effective cross section of $\gamma\gamma \rightarrow \ell_i \bar{\ell}_j$. In the optimum case, it can be written as [28]

$$\sigma_{\gamma\gamma \rightarrow \ell_i \bar{\ell}_j}(s) = \int_{\sqrt{a}}^{x_{max}} 2zdz \hat{\sigma}_{\gamma\gamma \rightarrow \ell_i \bar{\ell}_j}(s_{\gamma\gamma} = z^2s) \int_{z^2/x_{max}}^{x_{max}} \frac{dx}{x} F_{\gamma/e}(x) F_{\gamma/e}\left(\frac{z^2}{x}\right) \quad (24)$$

where $F_{\gamma/e}$ denotes the energy spectrum of the back-scattered photon for the unpolarized initial electron and laser photon beams given by

$$F_{\gamma/e}(x) = \frac{1}{D(\xi)} \left[1 - x + \frac{1}{1-x} - \frac{4x}{\xi(1-x)} + \frac{4x^2}{\xi^2(1-x)^2} \right] \quad (25)$$

with

$$D(\xi) = \left(1 - \frac{4}{\xi} - \frac{8}{\xi^2}\right) \ln(1+\xi) + \frac{1}{2} + \frac{8}{\xi} - \frac{1}{2(1+\xi)^2}. \quad (26)$$

Here $\xi = 4E_e E_0/m_e^2$ (E_e is the incident electron energy and E_0 is the initial laser photon energy) and $x = E/E_E$ with E being the energy of the scattered photon moving along the initial electron direction. The definitions of parameters ξ , $D(\xi)$ and x_{max} can be found in Ref.[28]. In our numerical calculation, we choose $\xi = 4.8$, $D(\xi) = 1.83$ and $x_{max} = 0.83$.

IV. THE PGB PAIR PRODUCTIONS IN pp , e^+e^- AND $\gamma\gamma$ COLLISIONS

In this section, we study cross sections for the double PGB production processes $gg \rightarrow \pi_t^+\pi_t^-, \pi_t^0h_t^0, \pi_t^0\pi_t^0, h_t^0h_t^0, q\bar{q} \rightarrow \pi_t^+\pi_t^-, \pi_t^0h_t^0, \pi_t^0\pi_t^0, h_t^0h_t^0, e^+e^- \rightarrow \pi_t^+\pi_t^-, \pi_t^0h_t^0$, and $\gamma\gamma \rightarrow \pi_t^+\pi_t^-, \pi_t^0h_t^0, \pi_t^0\pi_t^0, h_t^0h_t^0$. Since the signals of these processes as well as their corresponding backgrounds are not the same, we will analysis these processes separately. Throughout this paper, we take $m_t = 173$ GeV [25], $m_W = 80.38$ GeV, $m_Z = 91.19$ GeV [23], $\alpha_s(m_Z) = 0.118$ and neglect bottom quark mass as well as charm quark mass.

As for the TC2 parameters, we will consider the masses of the scalars equal to each other, i.e. the masses of the top-pions, neutral and charged, denoted as m_π when not considering the difference between them. Considering the discussion in the previous section, we will take m_π and K_{UR}^{tc} as the free parameters and assume m_π are in the range $200 - 600$ GeV, $K_{UR}^{tc} = 0.1 - 0.4$.

A. At The LHC

The parton processes $gg \rightarrow \pi_t^+ \pi_t^-, \pi_t^0 h_t^0, \pi_t^0 \pi_t^0, h_t^0 h_t^0, q\bar{q} \rightarrow \pi_t^+ \pi_t^-, \pi_t^0 h_t^0, \pi_t^+ \pi_t^0, h_t^0 h_t^0$ can be produced at the LHC, with the feynman diagrams shown in Fig.1 and Fig.4. To relatively know them, we here, firstly, discuss the contributions from every single parton channel though, actually, we can not distinguish the initial states, i.e, we will firstly discuss the gg fusion and the $q\bar{q}$ annihilation processes, respectively, and then sum them all together to see the total contributions.

By contrast to the lepton collider, the situation would be deteriorated at the hadron colliders such as LHC, however, on other aspect, the production probability of the new physics particles at LHC may be much larger, so that the disadvantage caused by background contamination may be compensated, which is proven in the following discussions.

1. $gg \rightarrow \pi_t^+ \pi_t^-$ and $gg \rightarrow \pi_t^0 h_t^0, \pi_t^0 \pi_t^0, h_t^0 h_t^0$

Due to the interactions in Eq.(7), the PGB pair production processes can proceed through various parton processes at the LHC, as shown in Fig.1, in which those obtained by exchanging the two external gluon lines are not displayed here.

Note that the processes consist of the box diagrams and the trilinear scalar coupling [29], just shown as Fig.1(a)(c) and (b)(d). The box contribution of the cross sections, however, is dominant since, firstly, in the s-channel contribution, the center of mass depress the production rate. Secondly, note that the $\pi_t^+ t \bar{b}$ coupling strength, $Y \sim \frac{m_t}{F_t} \frac{\sqrt{v_W^2 - F_t^2}}{v_W} \sim 3$, so we can imagine that one expects they may induce larger contributions to the relevant processes. Finally, the trilinear scalar coupling, i.e., the s-channel contribution is a two-loop diagram, as was expected, the contribution should be smaller than that of the one-loop contribution, i.e, the box diagram. The two contributions, we have calculated, are very small, less than 1 fb, and the interference contributions are small too, so we will not discuss them in the followings.

The production cross sections of the $\pi_t^+ \pi_t^-$ and $\pi_t^0 h_t^0, \pi_t^0 \pi_t^0, h_t^0 h_t^0$ of the gg fusion are plotted in Figs.2, 3 for $\sqrt{s} = 7, 14$ TeV and $K_{UR}^{tc} = 0.15, 0.35$, as functions of the top-pion mass m_π , assuming the top-higgs mass, $m_h = m_\pi$. From which, we can see the cross section of this process is quite large, about 1 pb in most of the parameter space and, as was expected, the production rate decreases with the increasing top-pion mass since the phase space are depressed by the top-pion mass.

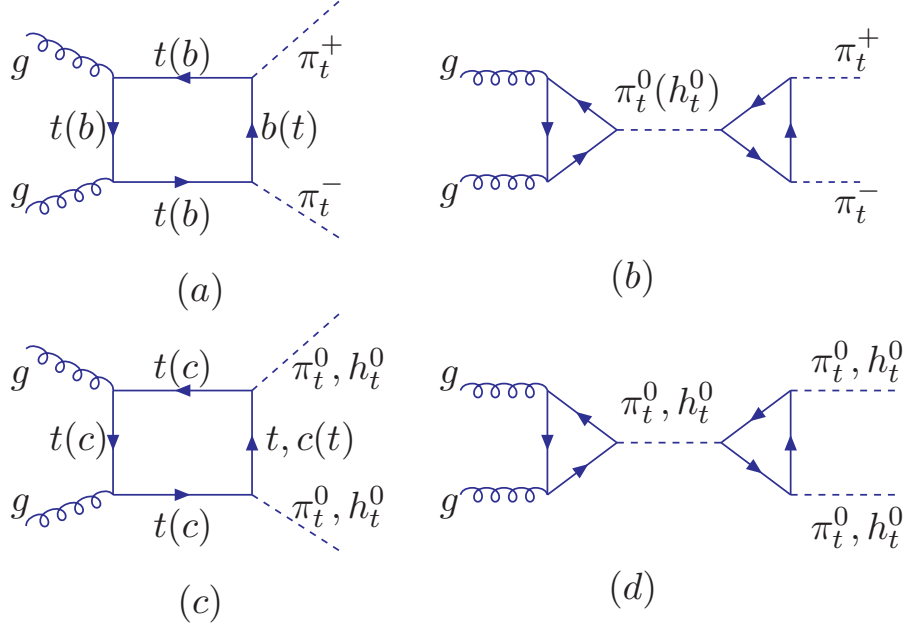


FIG. 1: Feynman diagrams for the PGB pair production at the LHC via gluon fusion parton level processes in the TC2 model. Those obtained by exchanging the two external gluon lines are not displayed here.

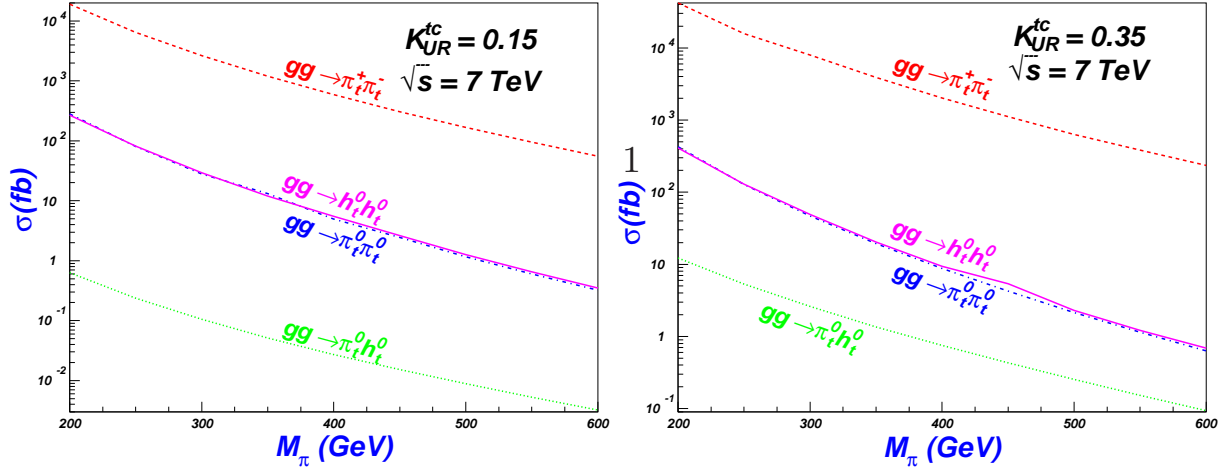


FIG. 2: The cross section σ of the processes $gg \rightarrow SS'$ as a function of the top-pion mass m_{π_t} with $K_{UR}^{tc} = 0.15$ and $K_{UR}^{tc} = 0.35$ and $\sqrt{s} = 7$ TeV.

In Figs.2, 3 we can also see the K_{UR}^{tc} dependence of the process $gg \rightarrow \pi_t^+ \pi_t^-$ is very weak since, in Fig.1 (a), the dominant contribution is the $\pi_t^+ t \bar{b}$ coupling, which is decided by factor $Y \sim 3$, irrelevant of the parameter K_{UR}^{tc} . Of course, the $\pi_t^+ \bar{b} c$ may also contribute by b, c quarks entering the loop, the production rate, however, are brought down by the $(K_{UR}^{tc})^4$ since the vertex $\pi_t^+ \bar{b} c$ appears twice in the loop diagrams. Even we take the optimum value

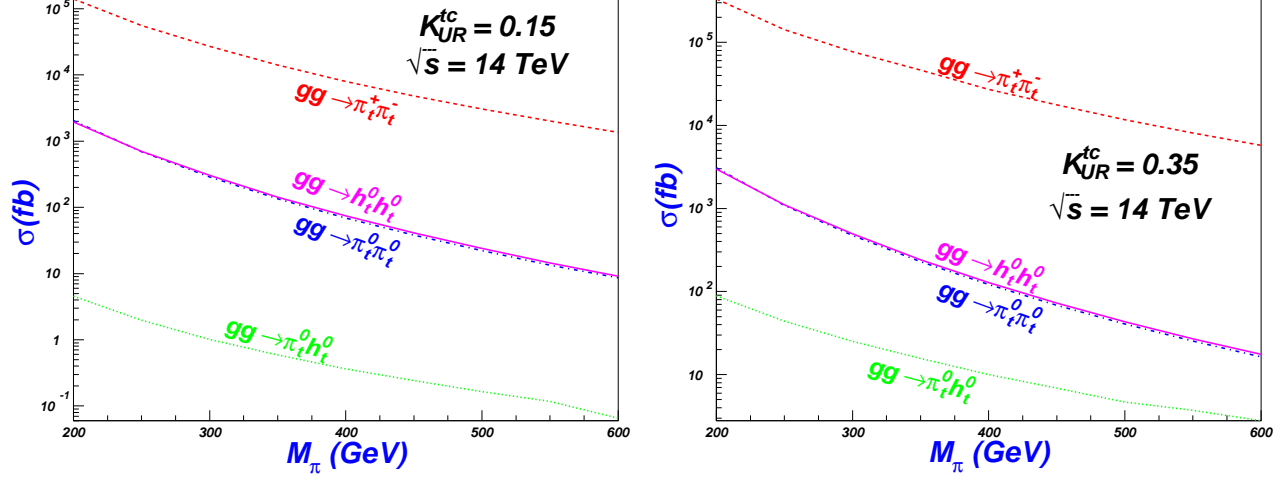


FIG. 3: Same as Fig.2, but for $\sqrt{s} = 14$ TeV.

of $K_{UR}^{tc} \sim 0.4$, the cross section will be $1/40$ depressed, so the cross section contributed by $bbbc$ and $cccb$ loop is very small. On this backgrounds, the interference terms between the loops contributed by t, b and c, b are also very small, less than 100 fb.

Similarly, the gluon gluon fusion processes of the $\pi_t^0 \pi_t^0$ and $h_t^0 h_t^0$ neutral scalar production, may be possess totally same behaviors since the couplings $\pi_t^0 t \bar{t}$ or $h_t^0 t \bar{t}$ are also independent of parameter K_{UR}^{tc} and the flavor changing couplings $\pi_t^0 t \bar{c}$ or $h_t^0 t \bar{c}$ contribute small since this type of couplings appears twice in the box diagrams, which can be seen clearly by comparing the Fig.2 and Fig.3 by different values of the parameter K_{UR}^{tc} .

But for the $gg \rightarrow \pi_t^0 h_t^0$ process, the situation will be different. Since the interaction between the CP-even and the CP-odd states may cancel out each other, the contributions from the all top quarks in the box loop may be much smaller than that of the $tttc$ and $ccct$ loop, so the terms with parameter K_{UR}^{tc} may play a great role. This is also verified by Fig.2 and Fig.3, from which we can see that the the rate of the $gg \rightarrow \pi_t^0 h_t^0$ is about two orders smaller than those of the $gg \rightarrow \pi_t^0 \pi_t^0$ and $h_t^0 h_t^0$, since in the latter the $tttt$ loop contributes large, and that the cross section of the $gg \rightarrow \pi_t^0 h_t^0$ is very sensitive to the K_{UR}^{tc} . For $\sqrt{s} = 14$ TeV, the cross section of the process $gg \rightarrow \pi_t^0 h_t^0$ arrives at 88 fb when $K_{UR}^{tc} = 0.35$, but only 4.6 fb when $K_{UR}^{tc} = 0.15$.

Summarily, For the the parameters K_{UR}^{tc} dependence, we can see from the fig.?? that the parameter it affects the rates of the production, and the cross section will increase with increasing K_{UR}^{tc} , but the effect is not too large. When the K_{UR}^{tc} increases form 0.15 to 0.35, the cross sections are in the same order. The rates of the $\pi_t^+ \pi_t^-$ production for $\sqrt{s} = 14$ TeV, for example, are 210 pb and 340 pb, for $K_{UR}^{tc} = 0.15$ and $K_{UR}^{tc} = 0.35$, respectively. That is understandable, since for the charged $\pi_t^+ \pi_t^-$ production, the $tttb$ and $bbbt$ contribution are primary, which is independent of the parameter K_{UR}^{tc} , while the $cccb$ and $bbbc$ loop are less important, which is related to the K_{UR}^{tc} , directly proportionally. The same cases occur for the $\pi_t^0 \pi_t^0$ and $h_t^0 h_t^0$ neutral production, $tttt$ contribution is larger than the $tttc$ and $ccct$ ones. But for the $gg \rightarrow \pi_t^0 h_t^0$, since the cancellation between the CP-even and CP-odd scalar

happen largely in the $tttt$ loop, the main contributions are from the $tttc$ and $ccct$ loops, so is is closely connected to the parameter K_{UR}^{tc} .

This discussion are also suitable for the processes $\gamma\gamma \rightarrow SS'$, which we will talk over in Sec. IV. C and the same conclusion will be talked about very simply.

2. $q\bar{q} \rightarrow \pi_t^+\pi_t^-$ and $q\bar{q} \rightarrow \pi_t^0h_t^0, \pi_t^0\pi_t^0, h_t^0h_t^0$ (the last two are for $c\bar{c}$ collision)

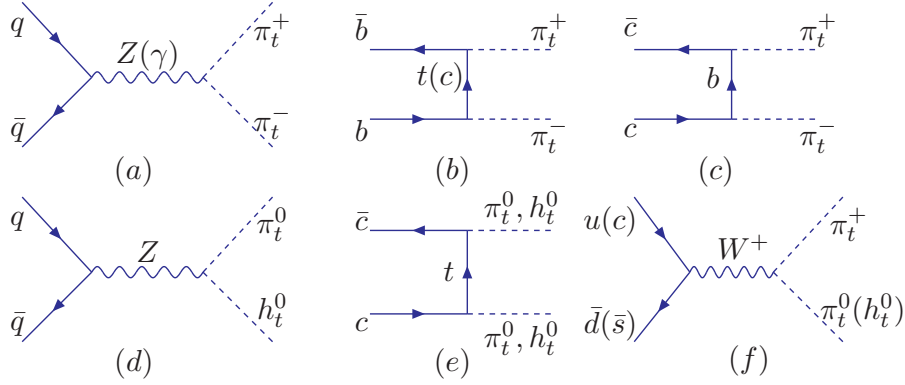


FIG. 4: Feynman diagrams for the PGB pair production at the LHC via quark annihilation parton level processes in the TC2 model and $q = u, d, s, c, b$ quarks.

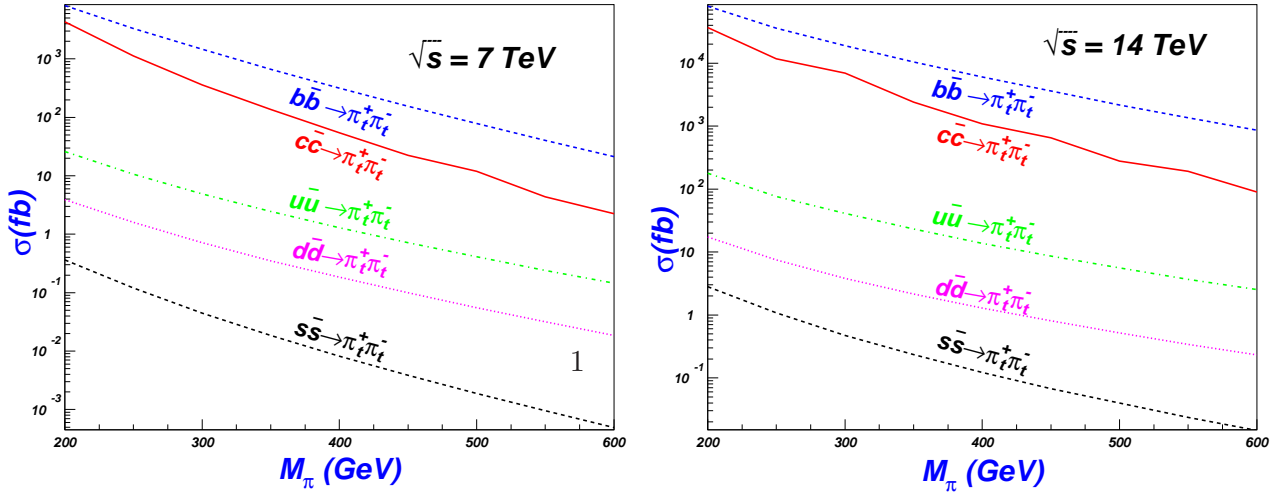


FIG. 5: The cross section σ of the processes $q\bar{q} \rightarrow \pi_t^+\pi_t^-$ as a function of the top-pion mass m_{π_t} with $\sqrt{s} = 7$ TeV and $\sqrt{s} = 14$ TeV, $q = u, d, s, c, b$.

Here, the t-channel neutral production $\pi_t^0h_t^0, \pi_t^0\pi_t^0, h_t^0h_t^0$ should have different cross sections with different couplings, but $\pi_t^0\pi_t^0, h_t^0h_t^0$ production are only contained by the t-channel processes, so we firstly take $\pi_t^0h_t^0$ as an example to compare with others, and the t-channel, i.e., $c\bar{c} \rightarrow \pi_t^0h_t^0, \pi_t^0\pi_t^0, h_t^0h_t^0$ will appear in the final of this section.

The s-channel processes such as (a)(d)(f) in Fig. 4, though the parton distribution functions could be larger for the $u\bar{u}$ and $d\bar{d}$ initial state, may be relatively small in view of the center-of-mass depression effects. At the same time, the t-channel coupling strengths are larger than those of the s-channel. In Fig. 4(b), For instance, the strengthen of $\pi_t^+ t\bar{b} \sim m_t/F_t \sim 3$ is much larger than that of $Z\pi_t^+\pi_t^-$, $Z\pi_t^0 h_t^0$ and $W\pi_t^+\pi_t^0$ in the s-channel processes, so no wonder the cross sections of the parton level processes like $u\bar{u}(d\bar{d}, s\bar{s}) \rightarrow Z \rightarrow \pi_t^+\pi_t^-(\pi_t^0 h_t^0)$ may be smaller than those of the others even with larger parton distribution functions. These can be seen clearly in Figs.5,7.

From Fig.5, we can also see that the largest channel of the processes $qq \rightarrow \pi_t^+\pi_t^-$ is the $b\bar{b} \rightarrow \pi_t^+\pi_t^-$ and $c\bar{c} \rightarrow \pi_t^+\pi_t^-$, which is easy to understand since, in Fig.5, the t-channel processes (b) and (c) are free of the center-of-mass depression and larger than others. The former, i.e., the process $b\bar{b} \rightarrow \pi_t^+\pi_t^-$, however, surpasses the process $c\bar{c} \rightarrow \pi_t^+\pi_t^-$, since the vertex $\pi_t^+ t\bar{b}$, different from $\pi_t^+ c\bar{b}$, is not associated with the K_{UR}^{tc} and not reduced by it.

But for the neutral scalar production via the $q\bar{q}$ collision, there is only one t-channel contribution in Fig.4 (e) since flavor changing neutral couplings induced by the neutral scalars π_t^0 and h_t^0 are small $\sim m_q$ (m_q is the quark mass) [3], except the $\pi_t^0(h_t^0)t\bar{c}$ coupling $\sim m_t$ with the large top quark mass, which appears in the t-channel of the $c\bar{c} \rightarrow \pi_t^0 h_t^0$.

For the neutral scalar production induced by the $q\bar{q}$ collision, the t-channel contribution is the largest when the production rates are not depressed too much by the factor K_{UR}^{tc} , about 100 fb and the other processes are smaller and have different cross sections. What makes the difference among them is only, if we neglect the masses of the quarks u, d, c, s, b , the parton distribution function in the proton, so it is naturally to see that $\sigma(u\bar{u}) > \sigma(d\bar{d}) > \sigma(s\bar{s}) > \sigma(b\bar{b})$.

Figs.6, 7 also shows m_π dependence of the cross section for $K_{UR}^{tc} = 0.15$ and 0.35, respectively. Comparing Fig.5 and Figs.6, 7, we can see that, in the latter, the cross sections becoming smaller, especially the t-channel processes $c\bar{c} \rightarrow \pi_t^+\pi_t^-$ and $c\bar{c} \rightarrow \pi_t^0 h_t^0$, about 1/30 of the former. That is easy to understand since the in the amplitudes the $\pi_t^+ b\bar{c}$ and $\pi_t^0 t\bar{c}$ or $h_t^0 t\bar{c}$ vertex, $\sim K_{UR}^{tc}$ appears twice, so the cross sections decrease $(0.15/0.35)^4 \sim 1/30$. But for process $b\bar{b} \rightarrow \pi_t^+\pi_t^-$, when we take $K_{UR}^{tc} = 0.15$, the depression rate is only 1/2, that is because in this process, when the intermediate particle is top quark in Fig.4(b), the contribution is dominant and the coupling $\pi_t^+ t\bar{b} \sim \frac{m_t}{F_t} \frac{\sqrt{V_W^2 - F_t^2}}{V_W}$ is irrelevant to the depression parameter K_{UR}^{tc} , so the rate is not sensitive to it too much.

Note that, for the neutral scalar productions, in Fig.6, $\sigma(u\bar{u} \rightarrow \pi_t^0 h_t^0) > \sigma(c\bar{c} \rightarrow \pi_t^0 h_t^0)$, which is opposite to the situation of Fig.7. This also shows that the $c\bar{c} \rightarrow \pi_t^0 h_t^0$ decreases with the decreasing K_{UR}^{tc} and more simultaneously, the process $u\bar{u} \rightarrow \pi_t^0 h_t^0$ is not related to the parameter K_{UR}^{tc} . Actually, all the s-channel processes in Fig.4(a),(d), are immune to the depression parameter K_{UR}^{tc} . So the weak advantage of the $\sigma(c\bar{c} \rightarrow \pi_t^0 h_t^0)$ over $\sigma(u\bar{u} \rightarrow \pi_t^0 h_t^0)$ will fade away with the decreasing K_{UR}^{tc} .

We also see from Fig.5 and Figs.6,7 that the charged scalar pair productions are much larger than the neutral ones with the same parameters, i.e, the top-pion mass m_π and K_{UR}^{tc} . The rate of $c\bar{c} \rightarrow \pi_t^+\pi_t^-$, for example, is about two orders larger than that of the $c\bar{c} \rightarrow \pi_t^0 h_t^0$,

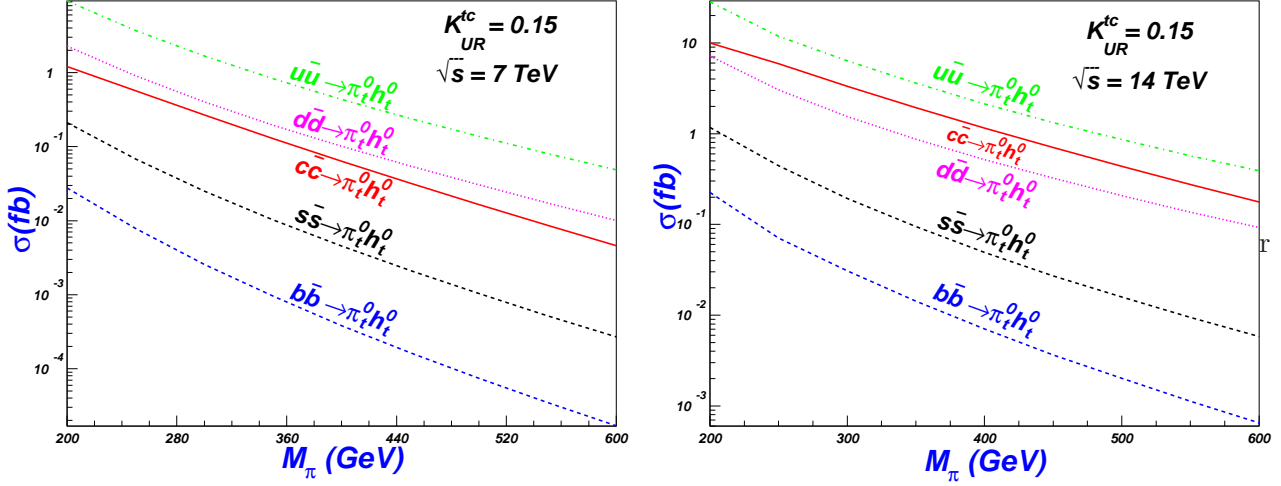


FIG. 6: The cross section σ of the processes $q\bar{q} \rightarrow \pi_t^0 h_t^0$ as a function of the top-pion mass m_{π_t} with $K_{UR}^{tc} = 0.15$ and $K_{UR}^{tc} = 0.35$ and for $\sqrt{s} = 7$ TeV, $q = u, d, s, c, b$.

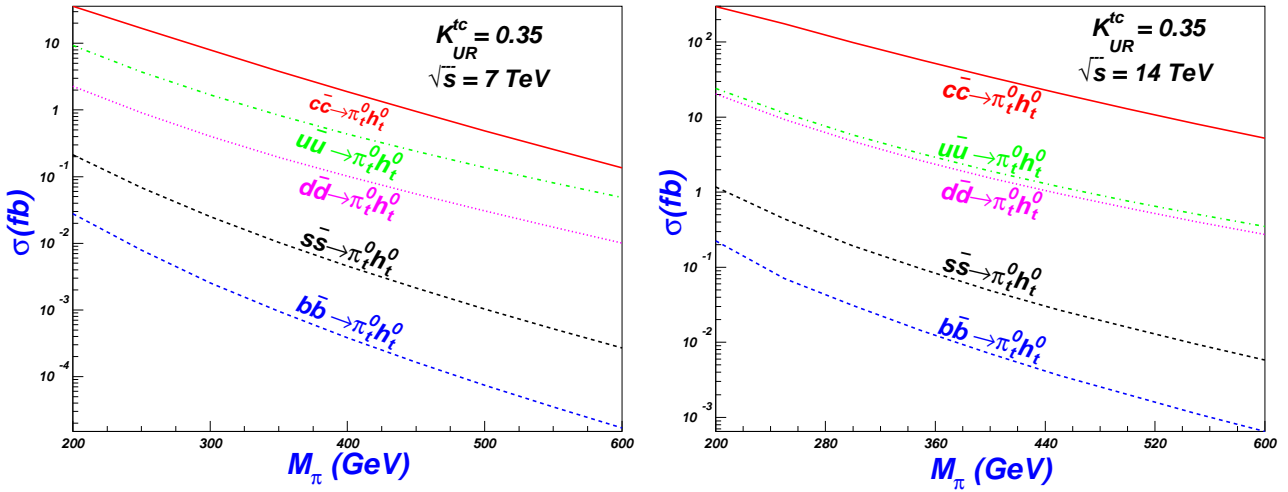


FIG. 7: Same as Fig.5, but for $\sqrt{s} = 14$ TeV.

which is simple to understand since the $\pi_t^+ t \bar{b}$ is free of the K_{UR}^{tc} depression and for $\pi_t^0(h_t^0)t\bar{c}$ that is not the truth.

We here only discussion the neutral pair production $\pi_t^0 h_t^0$, while for the $\pi_t^0 \pi_t^0$ and the $h_t^0 h_t^0$ production, the final particles are identical particles, due to identical particle statistics, the cross section of them would each be equal to $(1/2)^2$ of the $\pi_t^0 h_t^0$ cross section with the same scalar masses, considering the same coupling strength.

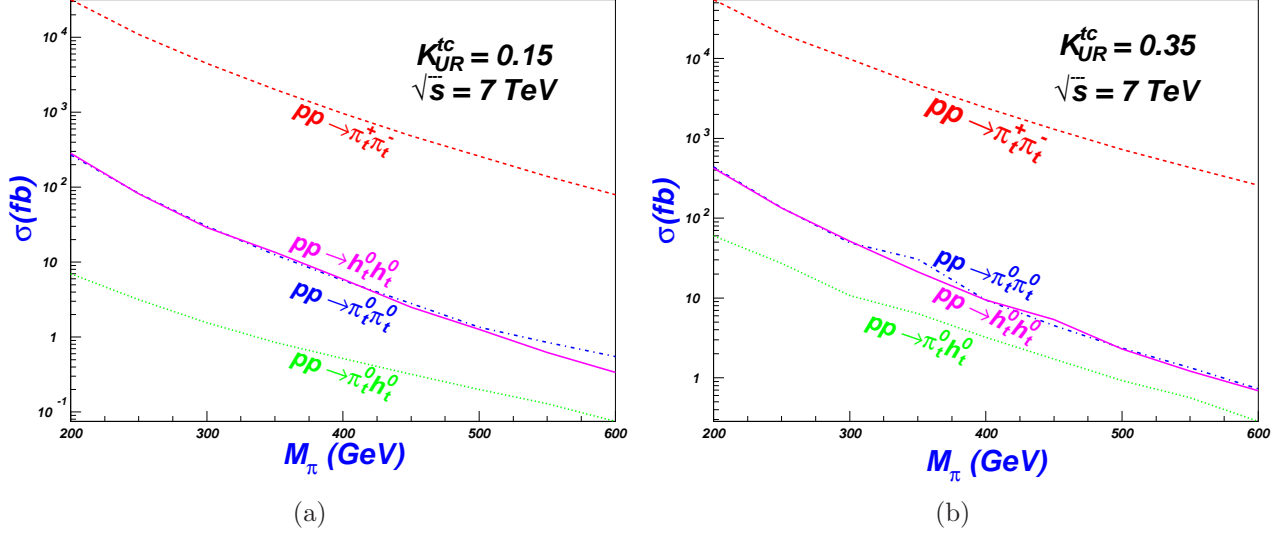


FIG. 8: The total cross section σ of the processes $p\bar{p} \rightarrow SS'$ as a function of the top-pion mass m_{π_t} with $\sqrt{s} = 7$ TeV and for $K_{UR}^{tc} = 0.15, 0.35$.

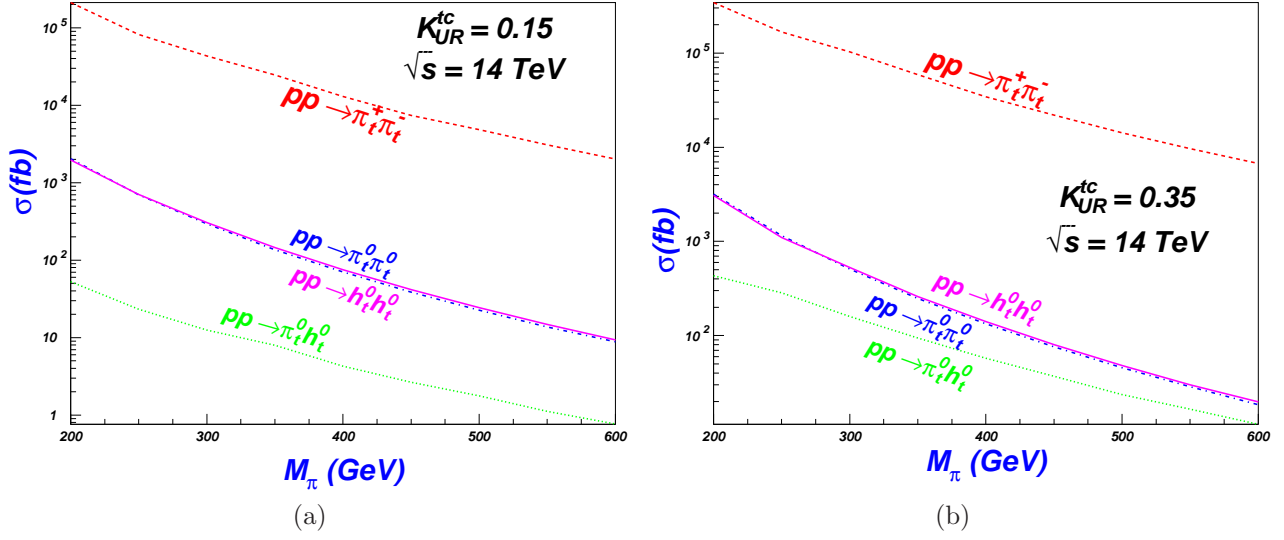


FIG. 9: Same as Fig.8, but for $\sqrt{s} = 14$ TeV.

3. The total contribution for the $\pi_t^+ \pi_t^-$ and $\pi_t^0 h_t^0, \pi_t^0 \pi_t^0, h_t^0 h_t^0$ at the LHC

Here we sum all the contributions, just shown as Fig.8 and Fig.9. From which we can see the total production rate of the charged top-pions is related to the top-pion mass and the center-of-mass and the production probability is larger than 6709 fb when the center-of-mass $\sqrt{s} = 14$ TeV and larger than 79 fb when $\sqrt{s} = 7$ TeV for $m_{\pi} = 600$ GeV. While for the neutral production of $pp \rightarrow h_t^0 h_t^0$ and $\pi_t^0 \pi_t^0$, the cross sections are about 2-3 orders smaller than the charged one. The cross section of the $h_t^0 h_t^0$ final state, for example, is about 3 pb for $m_{\pi} = 200$ GeV and $\sqrt{s} = 14$ TeV, while for the charged one, the rate can arrive at 340

pb.

We also see that the rates of the processes $pp \rightarrow h_t^0 h_t^0$ and $\pi_t^0 \pi_t^0$, are 1 – 2 orders larger than that of the $pp \rightarrow \pi_t^0 h_t^0$, which is because, in these productions, the gg fusion contributes most, while $q\bar{q}$ collision does not change the trend.

We can also see that K_{UR}^{tc} dependence is also almost the same as that of the gg fusion for every channel, which proves again that the gg fusion contributes largely.

$$4. \quad u\bar{d}(c\bar{s}) \rightarrow \pi_t^+ \pi_t^0 (h_t^0)$$

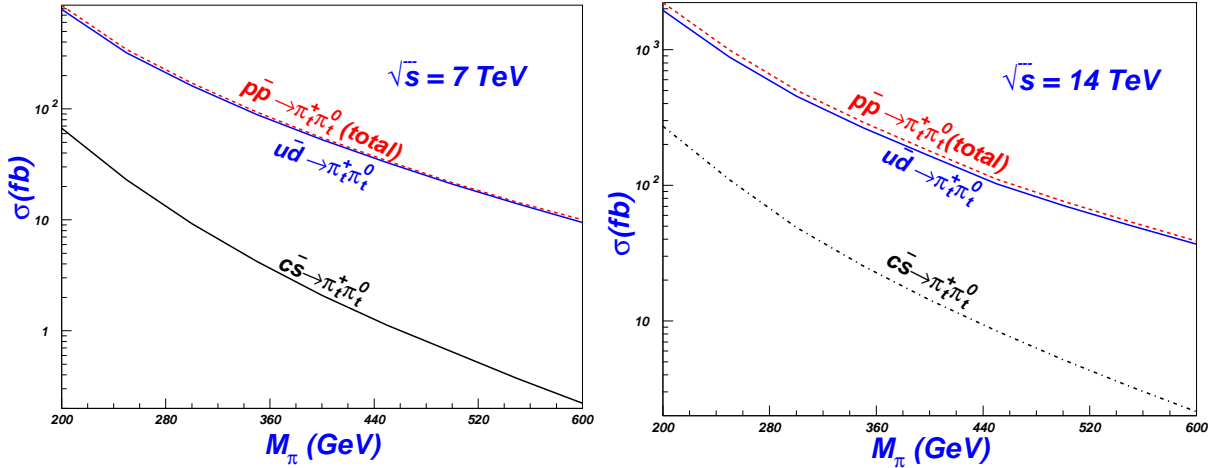


FIG. 10: The cross section σ of the processes $u\bar{d} \rightarrow \pi_t^+ \pi_t^0$ and $c\bar{s} \rightarrow \pi_t^+ \pi_t^0$ as a function of the top-pion mass m_{π_t} with $\sqrt{s} = 7$ TeV and $\sqrt{s} = 14$ TeV .

From Table I, we find the $W^{-\mu} h_t^0 \pi_t^+$ and $W^{-\mu} \pi_t^0 \pi_t^+$ couplings, which makes the one charged scalar and one neutral scalar, i.e, $\pi_t^+ \pi_t^0 (h_t^0)$, associated production possible at the LHC. The difference of the coupling strength of the $W^{-\mu} h_t^0 \pi_t^+$ and $W^{-\mu} \pi_t^0 \pi_t^+$ is only that in the $\pi_t^+ \pi_t^0 (h_t^0)$ coupling, there is an extra v_T/v factor, with $v_T = 241$ GeV and $v = 246$ GeV, the electroweak scale. So the coupling strength is almost the same, and the production rates of the $h_t^0 \pi_t^+$ and $\pi_t^0 \pi_t^+$ are taken as the same. From Fig.10, we can see the cross section can arrive to thousands of fb in most of the parameter spaces. Considering the special final states, this production may be interesting. We sum all the contributions and compare them together with that of every channel and find, from Fig.10, that the $u\bar{d}$ initial state contributes vast majority of the total contribution (the sum of that of the $u\bar{d}$ and the $c\bar{s}$) so that the two curves of the total and the $u\bar{d} \rightarrow \pi_t^+ \pi_t^0 (h_t^0)$ almost coincide with each other, which is easy to understand since the parton distribution function for the first generation is much larger than the others.

5. Backgrounds Analysis at the LHC

For final state $\pi_t^+ \pi_t^-$ at the LHC, the charged top-pions π_t^+ decays to $t\bar{b}$ and $c\bar{b}$ with the branching ratio about 70% and 30%[30], respectively. We assume the top-pions decaying to $t\bar{b}$, and top quark to b quark, charged lepton and the missing energy, i.e. the $4b + 2l + \cancel{E}$ signal² with \cancel{E} , the missing energy, so the mainly SM backgrounds are $pp \rightarrow WWZjj$ (with Z to $b\bar{b}$), $WWZZ$ (with one Z to $b\bar{b}$, the other to jj), $WWhh$, $t\bar{t}W$ (with W to two jets) and $WWb\bar{b}jj$, where h decays to $b\bar{b}$ and the $W \rightarrow l \cancel{E}$. Of course, the signal cross sections would be reduced by the branching ratios, $70\% \times 70\% \times 1/6 \times 1/6$.

The background cross-sections of the first three processes, i.e, $WWZjj$, $WWZZ$ and $WWhh$ are quite small since there are more than 3 QED vertexes which depress the strength. Considering the branching ratio of W and Z , the cross sections are at the level of several tens of fb, so they are negligible in the background discussion. For $pp \rightarrow t\bar{t}W$, the production rate, about 500 fb, similarly, the branching ratio of W decaying to hadrons, $1/3$, $t \rightarrow l \cancel{E}b$, $1/6$, then signal is about 4.6 fb, which is small contrast to the signal. As for the process $pp \rightarrow WWb\bar{b}jj$, quite large, about 437 pb, multiplying by the W branching ratios, 12 pb. To depress it, we apply, first, we can ask the transverse momentum cut $p_T^j > 20$ Gev, since in the signal, the transverse momentum of the jets, which are from the top-pion, are large, while the transverse momentum of the jets in the production $pp \rightarrow WWb\bar{b}jj$, are much smaller. So the background will be cut down largely, without losing much signatures at the same time. Secondly, the top-pion mass top quark mass reconstruction will be powerful to depress the background since in the signal the Wb comes from the top quark while in the background, it is not the true case. For these two means, we believe that the signal will not be reduced too much, such as 80% preserving, while the background may be depressed very much. we, based on the discussion above, here draw the conclusion that the signal cross sections arriving at 1000 fb may be observable at the LHC. Nevertheless, the discussion here is so crudely, and the precision are far beyond control. We will, in the next work, debate the observability at length.

Another final states at the LHC, $\pi_t^0 h_t^0$, $\pi_t^0 \pi_t^0$ and $h_t^0 h_t^0$, have same signature since the neutral bosons π_t^0 and the h_t^0 decay to the same states. If we assume the two final scalars decaying to $t\bar{c}$, the semileptonic decay of both top (or anti-top) quarks give rise to a signal of like-sign dilepton plus two b-jets, i.e., $\ell^\pm \ell^\pm + 2$ b-jets ($\ell = e, \mu$), so the signal is like-sign dilepton plus two b-jets, i.e., $\ell^\pm \ell^\pm + 2$ b-jets + 2 jets ($\ell = e, \mu$). Since we assume only two bottom quarks are tagged, the signal is the same as the charged top-pion pair production. Therefore the neutral and charged scalar pair production have same SM backgrounds. So is the charged and the neutral associated production $\pi_t^+ h_t^0$ and $\pi_t^+ \pi_t^0$.

Especially, the neutral top-pion or top-higgs pair final states can yield a like-sign dilepton signal, which is very exciting. To be specific, the flavor-changing decay of π_t^0 or h_t^0 will lead $1/2$ to $t\bar{c}$ and $1/2$ to $\bar{t}c$, so that the neutral pair leptonic decays will be 25% $l^+ l^+$, 25% $l^- l^-$,

² Actually, usually only 2 bottom quarks are tagged, so the signal is $2b + 2l + 2j + \cancel{E}$.

and 50% l^+l^- . This is exciting because the dominant $t\bar{t}jj$ background has only opposite-sign leptons.

To draw a very crudely conclusion, for an integrated luminosity 100 fb^{-1} at the LHC, the scalar pair production cross sections of 1000 fb may be the lower limit of the observability.

B. $e^+e^- \rightarrow \pi_t^+\pi_t^-$ and $e^+e^- \rightarrow \pi_t^0h_t^0$ at the ILC

At the ILC, PGB pair production carried on by the processes $e^+e^- \rightarrow \pi_t^+\pi_t^-$ and $e^+e^- \rightarrow \pi_t^0h_t^0$, the feynman diagrams of which are shown in Fig.11.

The advantage of analyzing such processes at the ILC is obvious that the hadronic background is very suppressed and the amount of signals may be practically observable. The calculation of the production at the e^+e^- collision is relatively simple compared to the case for hadron colliders because there is no QCD correction and moreover, there does not exist the complicated infrared divergence which needs to be properly dealt with.

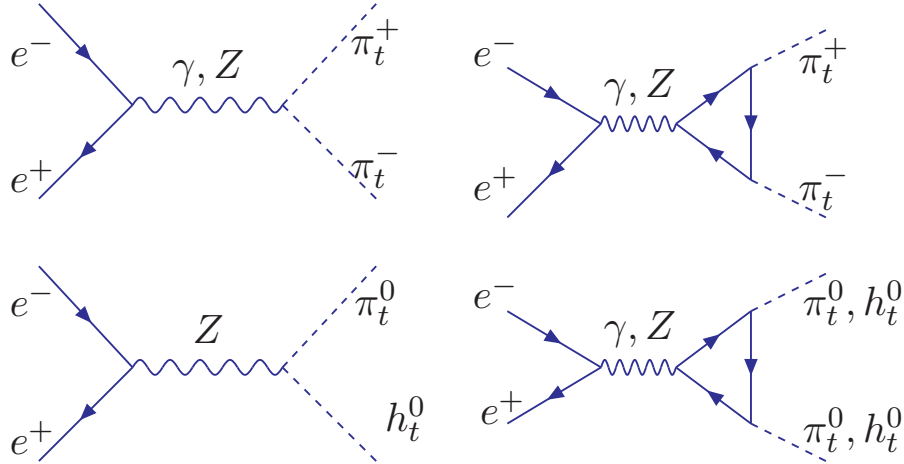


FIG. 11: Feynman diagrams for the PGB pair production at the ILC via electron positron collision processes in the TC2 model.

The cross sections of the two productions $\pi_t^+\pi_t^-$ and $\pi_t^0h_t^0$ can be seen in Fig.12, from which, we can see that the cross sections can reach 16.6 fb and 1.24 fb , for the charged and neutral production, respectively. It agrees on our expectation that the neutral production correction is smaller than that of the charged one. The reason is twofold is that for the neutral scalar production $e^+e^- \rightarrow \pi_t^0h_t^0$, at the tree-level the photon does not contribute and the $Z\pi_t^0h_t^0$ couplings is almost the same as the $Z\pi_t^+\pi_t^-$ coupling, which depresses the result.

As for the one-loop level of the two processes, the contributions are very small. The cross section of the charged pair production is smaller than 0.012 fb for $K_{UR}^{tc} = 0.35$, even smaller of the neutral production, less than 0.001 fb .

So we can estimate the contribution of the process $e^+e^- \rightarrow \pi_t^0h_t^0$ is smaller than that of the $e^+e^- \rightarrow \pi_t^+\pi_t^-$, which is verified in Fig.12(a)(b). The interference between tree level and

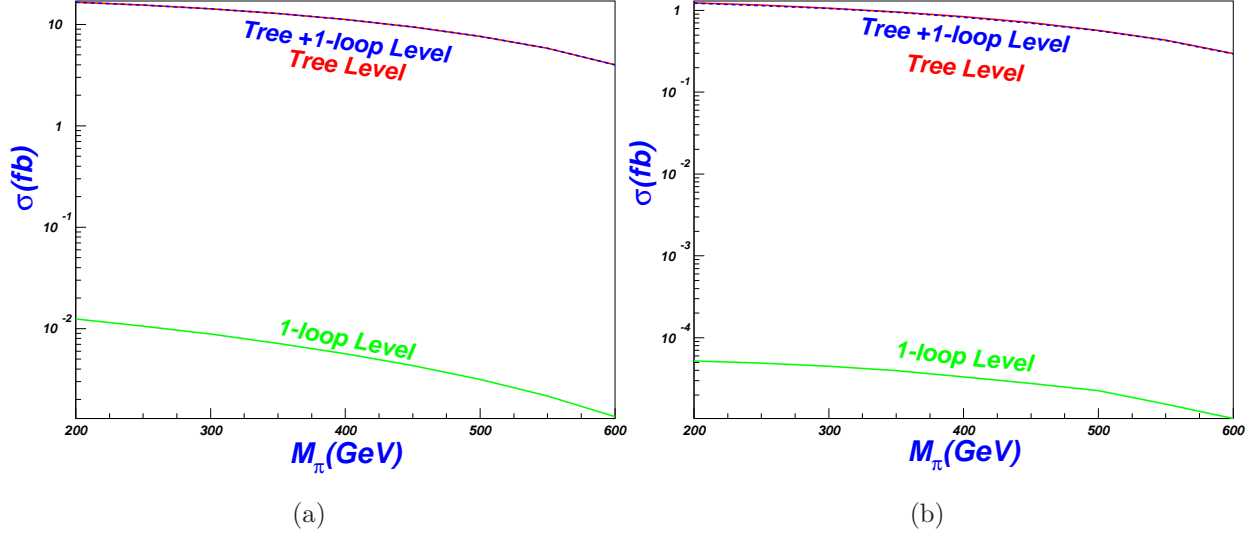


FIG. 12: Dependence of the cross section of $e^+e^- \rightarrow \pi_t^+\pi_t^-$ (a) and $e^+e^- \rightarrow \pi_t^0 h_t^0$ (b) on top-pion mass m_π for $\sqrt{s} = 1500$ GeV.

the one-loop level is also very small, which can be seen that the cross section hardly change whether we consider the one loop contribution or not.

Another thing is the parameter K_{UR}^{tc} dependence. Since the tree level contributions most and they are independent of the K_{UR}^{tc} , the cross section are almost the same with the changing K_{UR}^{tc} .

Note that the identical productions $\pi_t^0 \pi_t^0$ and $h_t^0 h_t^0$ are also considered and the rates are even small. Due to the shortage of the tree level contribution, both processes are proceeded at the one loop level. Moreover, the identical particles in the final states add a 1/2 factor, which even depress the cross sections. That was verified by our calculation, the production rates of the two identical processes, are less than 0.002 fb in the allowed parameter spaces. In view of the small contribution, we will here not discuss them in detail.

C. $\gamma\gamma \rightarrow \pi_t^+\pi_t^-$ and $\gamma\gamma \rightarrow \pi_t^0 h_t^0$, $\pi_t^0 \pi_t^0$, $h_t^0 h_t^0$ at the PLC

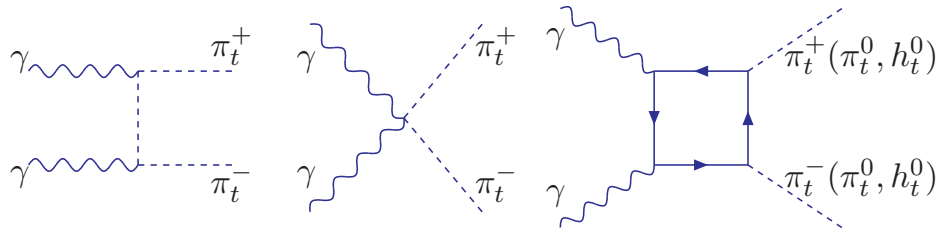


FIG. 13: The fenman diagrams of $\gamma\gamma \rightarrow \pi_t^+\pi_t^-$ and $\gamma\gamma \rightarrow \pi_t^0 h_t^0$ at the ILC.

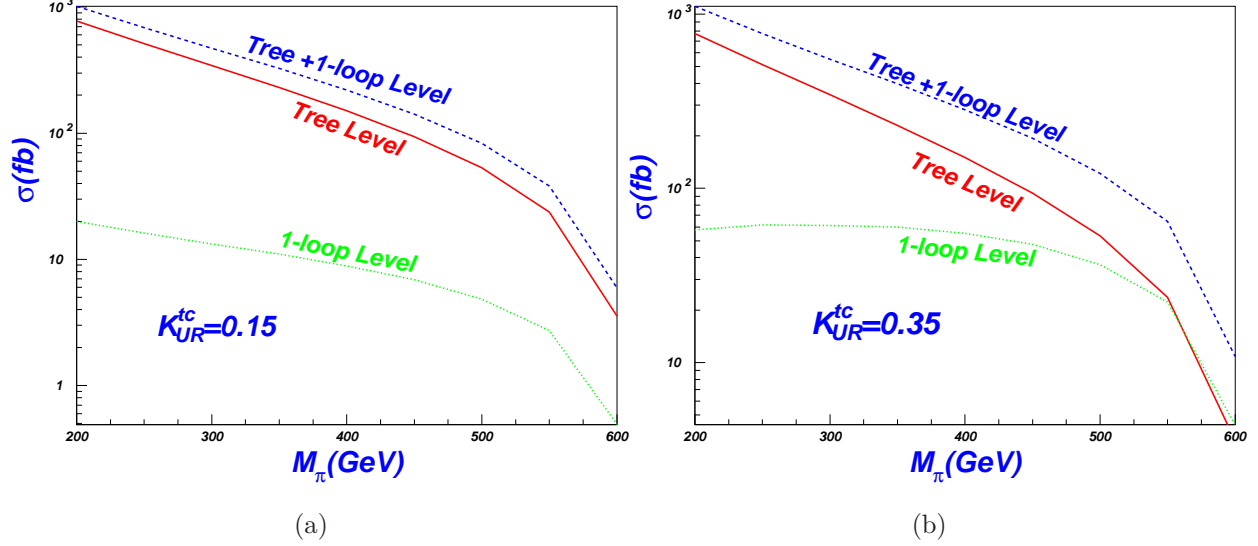


FIG. 14: Dependence of the cross section of $\gamma\gamma \rightarrow \pi_t^+ \pi_t^-$ on top-pion mass m_π with $\sqrt{s} = 1500$ GeV and for $K_{UR}^{tc} = 0.15$ (a), 0.35 (b).

This processes carry out through by the $\gamma\pi_t^+ \pi_t^-$ and $\gamma\gamma\pi_t^+ \pi_t^-$ couplings at the tree level, $\pi_t^+ t\bar{b}$ coupling at the 1-loop level, just shown in Fig.13. Since there is no new effects restricted to the TC2 model at the tree level, we also consider the 1-loop corrections, which are consisted of the typical TC2 couplings and one order smaller than the tree-level contribution, which can be seen clearly in Fig.14. Though the contributions may be enhanced by different diagrams, the loop depression are overwhelmingly larger so that the loop contribution is smaller that of the tree level.

From Fig.14 we can also see the production rates can reach one thousand fb and the cross sections decrease with the increasing top-pion mass m_π but larger than 1 fb almost in all the parameter space.

Compared the tree-level contribution of $e^+e^- \rightarrow \pi_t^+ \pi_t^-$ to that of the $\gamma\gamma \rightarrow \pi_t^+ \pi_t^-$, we find that the former is much smaller than the latter, the most important reason of which is that, for the $e^+e^- \rightarrow \pi_t^+ \pi_t^-$, the contribution is s-channel depression and the other process, i.e, $\gamma\gamma \rightarrow \pi_t^+ \pi_t^-$, is not infected with it.

Since the photon can't couple to the neutral scalars directly, and there is no tree level contribution, the neutral production process carry through out in the one-loop, just as the last figure in Fig.13. Fig.15 shows the dependence of the process $\gamma\gamma \rightarrow \pi_t^0 h_t^0, \pi_t^0 \pi_t^0, h_t^0 h_t^0$ on the m_π for $K_{UR}^{tc} = 0.15$ and 0.35 , respectively. We can see the cross section is smaller than 1 fb in quite a large parameter space and decrease with the increasing m_π from Fig.15.

From Fig.14 and Fig.15, we can also see that the scalar pair productions don't vary too much as the K_{UR}^{tc} . The reason is twofold. Firstly, At the tree level of charged production, it is unconcerned about the parameter K_{UR}^{tc} . Secondly, at the one-loop level of the charged and the scalar productions, the $ttt\bar{b}$, $b\bar{b}t\bar{t}$ and $ttt\bar{t}$ contributes largely, which are independent of K_{UR}^{tc} .

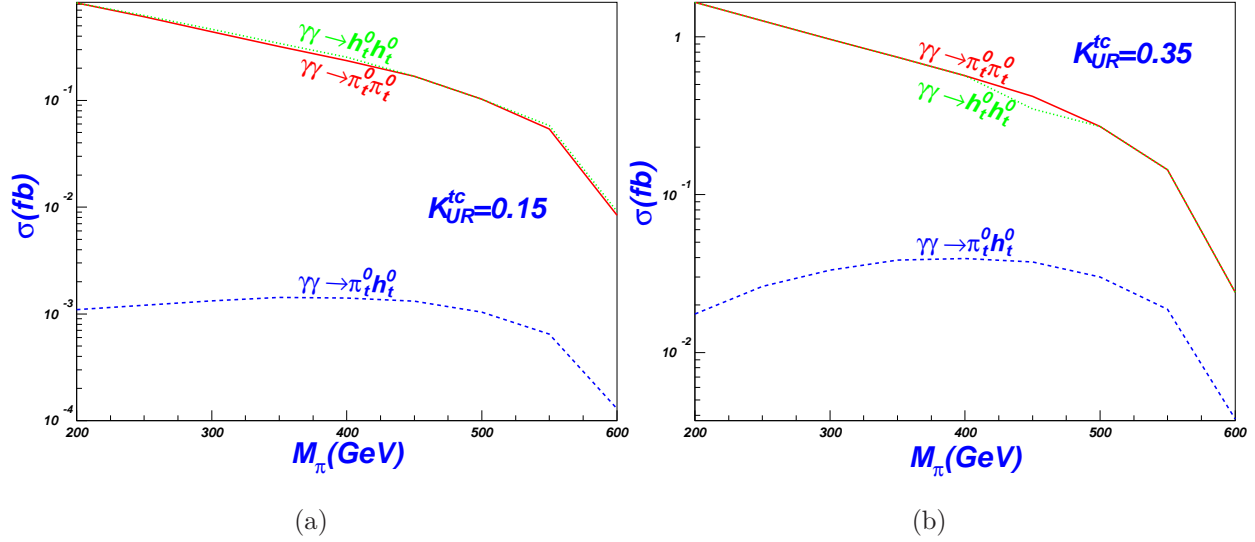


FIG. 15: Same as Fig.15, but for $\gamma\gamma \rightarrow \pi_t^0 h_t^0$, $\gamma\gamma \rightarrow \pi_t^0 \pi_t^0$ and $\gamma\gamma \rightarrow h_t^0 h_t^0$.

However, there is a little difference for the $\pi_t^0 h_t^0$, as the gg fusion processes. Since the larger CP-even and the CP-odd scalars cancel out, the cross section may change largely with varying K_{UR}^{tc} .

D. Simple Discussion of the ILC and the PLC Backgrounds Analysis

Given the predictions listed in Fig.12 and Fig.14, we now discuss their observability at the ILC. Firstly, for the final state $\pi_t^+ \pi_t^-$, the charged top-pions π_t^\pm still decays to $t\bar{b}$ with the branching ratio of 70% and the signal is the same as that at the LHC, i.e. the $2b + 2j + 2l + \cancel{E}$ signal. At the same time, for the $\pi_t^0 h_t^0$ final states, the neutral scalars decay to $t\bar{c}$, and the signal is also $2b + 2j + 2l + \cancel{E}$, the same as the charged production.

So for the two final states, the mainly SM ILC backgrounds will be $e^+e^- \rightarrow WWhh$, $WWZZ$, $WWZjj$, $t\bar{t}W$, $t\bar{t}jj$, the cross sections of the processes $WWhh$, $WWZZ$, $WWZjj$, $t\bar{t}W$, however, are below the order of 1 fb. The cross section of the last one, i.e., the $t\bar{t}jj$ production in the e^+e^- collision, are quite large, about 10fb.

Similarly, for the $\gamma\gamma$ collisions of the same final states $\pi_t^+ \pi_t^-$ and $\pi_t^0 h_t^0$, the main SM backgrounds is $\gamma\gamma \rightarrow WWhh$, $WWZZ$, $WWZjj$, $t\bar{t}W$, $t\bar{t}jj$, in which the cross section of the last one can arrive at 30 fb.

The backgrounds are in the same level of the signal, so we have to consider the depression. If the transverse momenta cuts, e.g. $p_t^j > 20$ GeV and the b-tagging skills, with 60% b-tagging efficiency and 1% mistagging, are employed, the backgrounds may be depressed very largely. Moreover, if the top-pion masses are reconstructed, the signal should be chosen out more clearly.

So we here assume that the pair PGB production at the ILC and the $\gamma\gamma$ collisions with a cross section larger than 10 fb may be observable at 95% C.L. for an integrated luminosity

of 100 fb^{-1} . Compared with the predictions in Fig.12 and Fig.14, one sees that TC2 model can enhance the production $e^+e^- \rightarrow \pi_t^+\pi_t^-$ and $\gamma\gamma \rightarrow \pi_t^+\pi_t^-$ and may be observable at the ILC in a large part of the parameter space.

V. SUMMARY AND CONCLUSION

We considered the PGB pair productions in the TC2 model, proceeding through $gg \rightarrow \pi_t^+\pi_t^-$, $gg \rightarrow \pi_t^0h_t^0$, $\pi_t^0\pi_t^0$, $h_t^0h_t^0$, $q\bar{q} \rightarrow \pi_t^+\pi_t^-$, $q\bar{q} \rightarrow \pi_t^0h_t^0$, $\pi_t^0\pi_t^0$, $h_t^0h_t^0$, $e^+e^- \rightarrow \pi_t^+\pi_t^-$, $e^+e^- \rightarrow \pi_t^0h_t^0$, $\gamma\gamma \rightarrow \pi_t^+\pi_t^-$, and $\gamma\gamma \rightarrow \pi_t^+\pi_t^-$, $\pi_t^0\pi_t^0$, $h_t^0h_t^0$ as a probe of the TC2 model. Since the backgrounds can be effectively suppressed by the scalar mass reconstruction, these processes can be used to probe the TC2 model. We found that these PGB pair productions in different collisions can play complementary roles in probing the TC2 model:

At the LHC, the cross section is large, and firstly we discussion the rates at the parton level, one by one, to compare their relative contribution.

- (1) For the $\pi_t^+\pi_t^-$ production at the LHC, the processes may be detectable when the cross sections reach 1000 fb, as discussed in the above section. For $gg \rightarrow \pi_t^+\pi_t^-$, the cross section can reach 1000 fb in most of the parameter spaces, which contributes large for this charged production. For $b\bar{b} \rightarrow \pi_t^+\pi_t^-$ and $c\bar{c} \rightarrow \pi_t^+\pi_t^-$, the cross sections can arrive at 1000 fb in most of the parameter spaces, which are also large at the LHC. For $u\bar{u} \rightarrow \pi_t^+\pi_t^-$, the cross section decreases with increasing m_π rapidly, though it is about 200 fb when $m_\pi = 200 \text{ GeV}$. When $m_\pi = 400 \text{ GeV}$, the cross section is only 13 fb. As the cross sections for other processes, $d\bar{d} \rightarrow \pi_t^+\pi_t^-$ and $s\bar{s} \rightarrow \pi_t^+\pi_t^-$ are even smaller. So the processes $u\bar{u}$, $d\bar{d}$, $s\bar{s} \rightarrow \pi_t^+\pi_t^-$ can't contribute much at the LHC in most of the parameter space.
- (2) The process $pp \rightarrow \pi_t^0\pi_t^0$ and $pp \rightarrow h_t^0h_t^0$ can arrive 2000 fb for $\sqrt{s} = 14 \text{ TeV}$, but with increasing m_π and decreasing \sqrt{s} , the production rate decreases rapidly. For example, when $\sqrt{s} = 7 \text{ TeV}$ and $m_\pi = 600 \text{ GeV}$, the productions are only about 0.5 fb.
- (3) The process $gg \rightarrow \pi_t^0h_t^0$ is closely connected to the parameter K_{UR}^{tc} . The cross section, however, is not too large. The cross section With $K_{UR}^{tc} = 0.35$ and $\sqrt{s} = 14 \text{ TeV}$, for example, is smaller than 430 fb. The $q\bar{q} \rightarrow \pi_t^0h_t^0$ is much smaller.
- (4) For the process $u\bar{d} \rightarrow \pi_t^+\pi_t^0$, the cross section is larger than 100 fb in most of the parameter space, while $c\bar{s} \rightarrow \pi_t^+\pi_t^0$, smaller than 100 fb in quite a large space, so the parton production of the $u\bar{d} \rightarrow \pi_t^+\pi_t^0$ contributes most in the $pp \rightarrow \pi_t^+\pi_t^0$ process.

The total cross sections σ (with all the initial states contribution summed and the final states summed) of the processes $p\bar{p} \rightarrow SS'$ as a function of the top-pion mass m_{π_t} with $\sqrt{s} = 7 \text{ TeV}$ and $\sqrt{s} = 14 \text{ TeV}$ and for $K_{UR}^{tc} = 0.15, 0.35$ are given in Fig.16. We can see from Fig.16 that the total cross sections decrease with the increasing top pion mass, and vary very slightly with the parameter K_{UR}^{tc} , since the charged production is dominant, which

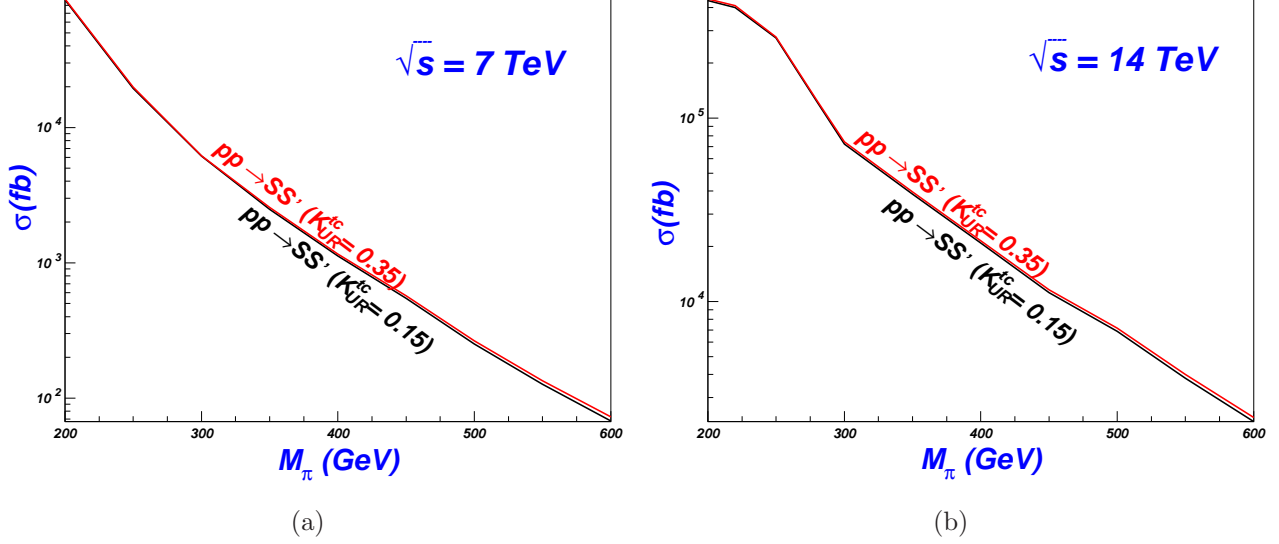


FIG. 16: The total cross section σ of the processes $p\bar{p} \rightarrow SS'$ as a function of the top-pion mass m_{π_t} with $\sqrt{s} = 7$ TeV and $\sqrt{s} = 14$ TeV and for $K_{UR}^{tc} = 0.15, 0.35$.

is free from the K_{UR}^{tc} . We can also see that the cross sections are quite large, about 1000 fb for $\sqrt{s} = 7$ TeV in a good case, much larger than 1000 fb for $\sqrt{s} = 14$ TeV in a large part.

According to the background analysis above, the total production $pp \rightarrow SS'$ may be detected at the LHC with quite a large possibility.

For the $\pi_t^+ \pi_t^-$ production at the ILC, the processes may be detectable when the cross sections reach 10 fb. For $e^+ e^- \rightarrow \pi_t^+ \pi_t^-$ and $\gamma\gamma \rightarrow \pi_t^+ \pi_t^-$, the cross section can reach 20 fb in most of the parameter spaces, which is possible to be detected at the ILC. Similarly, the processes $e^+ e^- \rightarrow \pi_t^0 \pi_t^0$ and $\gamma\gamma \rightarrow \pi_t^0 \pi_t^0$, below 10 fb in most of the parameter space, difficult to observe at the ILC if the signal are singled out. According to discussion above, however, the charged and the neutral productions have the same collider signature, so the total cross section at the ILC and the PLC may be both observable.

As a conclusion, as long as the top-pions are not too heavy, e.g., below 500 GeV, the productions might be detectable at the LHC, the ILC and the PLC. In general, the charged pion pair productions have larger possibility to be detectde since their couplings to $t\bar{b}$ are not suppressed by K_{UR}^{tc} . while for the neutral pion productions, the cross sections are closely connected to the parameter K_{UR}^{tc} . We see from the figures listed above that in a large part of the parameter space the cross sections of the scalar pair productions can reach the possible detectable level (1000 fb for the LHC and 10 fb for the ILC). Therefore, the pair productions of PGBs may serve as a good probe of the TC2 model.

Acknowledgments

We would like to thank J. J. Cao, Q. Yan, J. M. Yang, and S. Yang for helpful discussions. This work was supported by the National Natural Science Foundation of China under the

-
- [1] M. C. Gonzalez-Garcia and Y. Nir, *Rev. Mod. Phys.* **75**, 345(2003); V. Barger, D. Marfatia, and K. Whisnant, *Int. J. Mod. Phys E***12**, 569(2003); A. Y. Smimov, *hep-ph/0402264*.
 - [2] S. Weinberg, *Phys. Rev. D***13**(1976) 974; *ibid*, *D***19** (1979) 1277; L. Susskind, *Phys. Rev. D***20**, (1979) 2619; E. Farhi, L. Susskind, *Phys.Rept.***74**, (1981) 277.
 - [3] C. T. Hill, *Phys. Lett. B* **345**, 483 (1995); K. Lane and E. Eichten, *Phys. Lett. B* **352**, 383 (1995); K. Lane, *Phys. Lett. B* **483**, 96 (1998); G. Cvetič, *Rev. Mod. Phys.***71**, 513 (1999); C. T. Hill and E. H. Simmons, *Phys. Rept.* **381**, 235 (2003).
 - [4] G. Cvetič, *Rev. Mod. Phys.* **71**, 513 (1999); S. P. Martin, *Phys. Rev. D***46**, 2197 (1992); *Phys. Rev. D***45**, 4283 (1992), *Nucl. Phys. B* **398**, 359 (1993); M. Lindner and D. Ross, *Nucl. Phys. B* **370**, 30 (1992); R. Bonisch, *Phys. Lett. B***268**, 394 (1991); C. T. Hill, D. C. Kennedy, T. Onogi, H. L. Yu, *Phys. Rev. D***47**, 2940 (1993).
 - [5] See, e.g., G. Liu, et al., *Phys. Rev. D* **82**, 115032 (2010); *Chin. Phys. Lett.***26**, 101401 (2009); *Science China*, **53**, 1 (2010); *Commun. Theor. Phys.* **55**, 852 (2011); *Chin. Phys. C***32**, 697 (2008); J. Cao, et al., *Phys. Rev. D* **76**, 014004 (2007); *Phys. Rev. D* **75**, 075021 (2007); *Phys. Rev. D* **70**, 114035 (2004); H. J. Zhang, *Phys. Rev. D* **77**, 057501 (2008); X. L. Wang et al., *Phys. Rev. D* **50**, 5781 (1994); C. Yue, et al., *Phys. Lett. B* **496**, 93 (2000);
 - [6] ATLAS Collaboration, Technical Design Report, CERN-LHCC-99-15; CMS Collaboration, Technical Proposal, CERN-LHCC-94-38; G. Weiglein, et al., [LHC/LC Study Group], *hep-ph/0410364*.
 - [7] A. Cagil, *Nucl. Phys. B* **843**, 46 (2011); L. Wang, W. Wang, J. M. Yang, H. Zhang, *Phys. Rev. D* **76**, 017702 (2007); X.-F. Han, L. Wang, J. M. Yang, *Nucl. Phys. B* **825**, 222 (2010); T. Han, B. Mukhopadhyaya, Z. Si, K. Wang, *Phys. Rev. D* **76**, 075013 (2007); E. Asakawa, E. D. Harada, S. Kanemura, Y. Okada, K. Tsumura, *Phys. Rev. D* **82**, 115002 (2010); A. Gutierrez-Rodriguez, M. Hernandez-Ruiz, O. Sampayo, *Int. J. Mod. Phys. A***24**, 5299 (2009); W. Ma, C. X. Yue, Y. Z. Wang, *Phys. Rev. D* **79**, 095010 (2009).
 - [8] W. A. Bardeen, C. T. Hill and M. Lindner, *Phys. Rev. D* **41**, 1647 (1990); G. Cvetič, *Rev. Mod. Phys.* **71**, 513 (1999), *hep-ph/9702381*.
 - [9] T. Eguchi, *Phys. Rev. D* **14**, 2755 (1976).
 - [10] A. K. Leibovich and D. Rainwater, *Phys. Rev. D* **65**, 055012 (2002).
 - [11] R. S. Chivukula, B. Coleppa, H. E. Logan, A. Martin, E. H. Simmons, MSUHEP-110819; FERMILAB-PUB-11-386-T, *arXiv:1108.4000*.
 - [12] H. J. He and C. P. Yuan, *Phys. Rev. Lett.* **83**, 28 (1999); C. Balazs, H.-J. He, C.P. Yuan, *Phys.Rev. D***60** (1999) 114001; H.-J. He, S. Kanemura, C. P. Yuan, *Phys. Rev. Lett.* **89**, 101803 (2002); *Phys. Rev. D* **68**, 075010 (2003).
 - [13] A. K. Das and C. Kao, *Phys. Lett. B* **372**, 106 (1996).
 - [14] C. T. Hill and G. G. Ross, *Nucl. Phys. B* **311**, 253 (1988); *Phys. Lett. B* **203**, 125 (1988).

- [15] B. Balaji, *Phys. Rev. D* **53**, 1699 (1996) .
- [16] H. Pagels and S. Stokar, *Phys. Rev. D* **20**, 2947 (1979).
- [17] C. T. Hill, *Phys. Lett. B* **266**, 419 (1991).
- [18] G. Burdman, *Phys. Rev. Lett.* **83**, 2888 (1999).
- [19] R. S. Chivukula, B. A. Dobrescu, H. Georgi and C. T. Hill, *Phys. Rev. D* **59**, 075003 (1999); H.-J. He, C.T. Hill, T.M.P. Tait, *Phys.Rev. D* **65** (2002) 055006.
- [20] B. Balaji, *Phys. Lett. B* **393**, 89 (1997).
- [21] G. Burdman and D. Kominis, *Phys. Lett. B* **403**, 101 (1997); W. Loinaz and T. Takeuchi, *Phys. Rev. D* **60**, 015005 (1999).
- [22] C. T. Hill and X. Zhang, *Phys. Rev. D* **51**, 3563 (1995) C. Yue, Y. P. Kuang, X. Wang and W. Li, *Phys. Rev. D* **62**, 055005 (2000).
- [23] Particle Data Group, *J. Phys. G* **37**, 075021 (2010).
- [24] J. Cao, Z. Xiong and J. M. Yang, *Phys. Rev. D* **67**, 071701 (2003).
- [25] CDF Collaboration, *Phys. Rev. Lett.* **105**, 252001 (2010).
- [26] J. Pumplin, et al., *JHEP* **0207**, 012 (2002).
- [27] T. Hahn and M. Perez-Victoria, *Comput. Phys. Commun.* **118**, 153 (1999).
- [28] I. F. Ginzburg, *et al.*, *Nucl. Instrum. Meth. A* **219**, 5 (1984).
- [29] A. Doff, A. A. Natale, *Phys. Lett. B* **641**, 198 (2006).
- [30] X. Wang, W. Xu, L. Du, *Commun. Theor. Phys.* **41**, 737 (2004); C. Yue, Q. Xu, G. Liu, J. Li, *Phys. Rev. D* **63**, 115002 (2001).
- [31] E. L. Berger, C. B. Jackson, S. Quackenbush, G. Shaughnessy, arXiv:1107.3150; Carlo Oleari, Laura Reina, arXiv:1105.4488; R.K. Ellis, S. Veseli, *Phys. Rev. D* **60**, 011501 (1999).
- [32] W. S. Hou, G. L. Lin, C. Y. Ma and C. P. Yuan, *Phys. Lett. B* **409**, 344 (1997); G. L. Lin, hep-ph/9705424; F. Larios and F. Penunuri, *J. Phys. G* **30**, 895 (2004).
- [33] V. Barger, K. Cheung, T. Han and R. J. N. Phillips, *Phys. Rev. D* **42**, 3052 (1990).
- [34] A. Kulesza and W. J. Stirling, *Phys. Lett. B* **475**, 168 (2000).
- [35] Y. P. Gouz and S. R. Slabospitsky, *Phys. Lett. B* **457**, 177 (1999).
- [36] X. Wang, Q. Qiao and Q. Zhang, *Phys. Rev. D* **71**, 095012 (2005).
- [37] Q. Qiao, Z. Li, X. Li, X. Wang, *Commun. Theor. Phys.* **52**, 311 (2009).
- [38] A. Djouadi, W. Kilian, M. Muhlleitner, P.M. Zerwas, *Euro. Phys. J. C* **10**, 27 (1999); G. Belanger and F. Boudjema, *Phys. Lett. B* **288**, (1992) 201-209.
- [39] B. Sahin, *J. Phys. G* **36**, 025012 (2009).